Chapter **1**

Introduction and Fundamental Concepts

Chapter 1 focuses on the fundamentals of near-field thermal radiation. It provides a brief overview of the different modes of heat transfer before introducing the reader to near-field thermal radiation. At present none of the graduate-level text books on radiation heat transfer provide an in-depth second law analysis during radiative heat transfer. Hence a separation section on entropy generation and flow in radiative transfer has been provided in this chapter in Section 1.2. In Section 1.3, we introduce the concepts of near-field thermal radiation elucidating the differences from far-field radiation. Ray tracing techniques or the radiative transfer equation do not fully account for the origin of thermal emission and break down when

wave interference and diffraction become important at length scales comparable to wavelength of thermal radiation. As a result, near-field effects cannot be explained under such a framework and electric and magnetic fields need to be calculated from Maxwell's equations before the heat transfer can be determined. Detailed derivation of the electric and magnetic fields based on Maxwell's equations and Green's function formalism have been provided in this chapter for calculating the radiative heat transfer between two semi-infinite parallel plates. Salient features of near-field heat transfer like evanescent waves and photon tunneling have also been discussed in great detail. The last section in the chapter investigates the entropy generation during near-field heat transfer. While there have been a lot of publications predicting as well as measuring the near-field heat flux only a few studies have unambiguously provided accurate second law analysis of near-field thermal radiation. Hence the last section is very important for furthering the understanding of entropy generation in near-field thermal radiation with potential applications in alternate energy systems.

1.1 **HEAT TRANSFER FUNDAMENTALS**

Heat transfer is defined as the transfer of energy between two systems due to the temperature difference between them. The two systems could be solids, liquids, or gases and the transfer of energy always happens from media at higher temperature to those at lower temperature in keeping with laws of thermodynamics. Applications of heat transfer are abundant in everyday life from complex biological processes to industrial systems in both macro and micro/nano scale. Different heat transfer processes are referred to as modes. When heat transfer happens across a stationary medium due to temperature gradient, the corresponding heat transfer mode is referred to as conduction. The stationary medium can be solids, liquids, or gases. An example of conduction is the addition of insulation on hot water pipes in cold temperatures to prevent heat loss. Convective heat transfer refers to the heat transfer between the surface and a moving fluid and as such depends on both the velocity and temperature of the moving fluid. An example of convective heat transfer is the cooling of a cup of coffee by blowing air over it. The third mode of heat transfer is radiative heat transfer which takes place due to the emission and absorption of electromagnetic waves between different objects in the absence of any intervening medium. An example of radiative heat transfer is the energy transferred due to solar radiation. While conductive and convective heat transfer are proportional to the temperature difference, radiative heat transfer varies as the fourth power of temperature of the media.
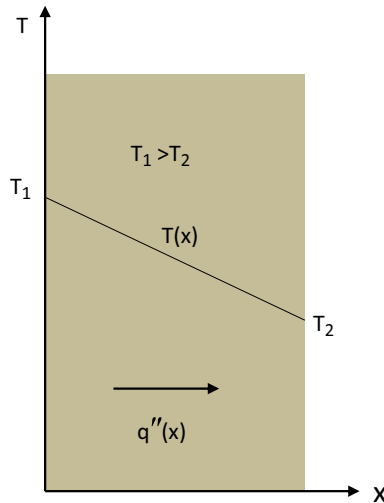
1.1.1 **Conduction**

Conduction or diffusion can be considered as the energy transfer from more energetic particles to less energetic particles inside a stable medium. The best way to understand conduction heat transfer is to think of a gas which occupies the space between two surfaces maintained at different temperatures. The gas is stationary and there is no bulk motion in the gas. Higher temperature implies more energetic molecules and greater random motion of the molecules. As the molecules collide there is exchange of energy from more energetic particles to less energetic particles. Consequently, energy is transferred from the high-temperature surface to the low-temperature surface in the direction of decreasing temperature.

Let us consider a 1D plane wall whose two surfaces are maintained at temperature T_1 and T_2 with a temperature distribution $T(x)$ inside the wall as shown in Fig. 1.1. The well-known Fourier's law states that the heat flux is proportional to the temperature gradient with the proportionality constant called thermal conductivity, ie,

$$q'' = -\kappa \nabla T \tag{1.1}$$

In the above equation, κ is the thermal conductivity of the medium across which the heat transfer takes place. The negative sign in Eq. (1.1) implies that the heat transfer happens in the direction of decreasing temperature gradient. q'' is the heat flux vector whose direction is always perpendicular to isotherms (equal temperature surface). For isotropic medium, thermal

■ **FIGURE 1.1** Schematic drawing of 1D heat conduction across a plane wall.

conductivity is independent of direction. However for anisotropic media such as thin films, nanowires, or multilayered media, the thermal conductivity depends on the direction along which it is measured. Notice the similarity of Eq. (1.1) to Ohm's law in electricity. For the 1D plane wall, the heat flux expression is given by $q''_x = -\kappa \frac{dT}{dx}$. After applying the boundary conditions of $T(0) = T_1$ and $T(L) = T_2$, the heat flux is then given by

$$q''_x = -\kappa \frac{(T_2 - T_1)}{L} \tag{1.2}$$

Note that Fourier's law provides the steady-state temperature distribution inside the medium. If we do a control volume analysis using an energy balance given by the following [1]

$$\dot{E}_{in} + \dot{E}_g - \dot{E}_{out} = \dot{E}_{st} \tag{1.3}$$

the transient temperature distribution in a homogeneous medium is then given by

$$\nabla \cdot (\kappa \nabla T) + \dot{q} = \rho c_p \frac{\partial T}{\partial t} \tag{1.4}$$

In Eq. (1.3), $\dot{E}_{in}$ is the transient energy inflow to the control volume, $\dot{E}_{out}$ is the transient energy leaving the system, $\dot{E}_g$ is the energy generated in the control volume per unit time, and $\dot{E}_{st}$ is the transient energy storage. In Eq. (1.4) ρc_p is the volumetric heat capacity. Typical thermal conductivities of metals are in the range of 100−1000 W/m K, alloys have thermal conductivities in the range from 10−100 W/m K, while insulators have conductivities on the order of 0.1 W/m K. Thermal conductivity of air is 0.0263 W/m K at room temperature. Note that the thermal conductivity is a function of temperature. Diamond has the highest thermal conductivity of 2300 W/m K of all natural materials. However, carbon nanotubes can have even higher thermal conductivity. On the other hand, graphene which is a one-atom thick layer of graphite has lateral conductivity of 5000 W/m K and can act as a very good heat spreader [2].

1.1.2 **Convection**

Convection heat transfer is the heat transfer from a solid to a fluid when the fluid is in bulk motion, which distinguishes it from conduction. Convection is composed of two modes diffusion (across the boundary of solid and fluid) and advection (bulk motion of the fluid). Consider Fig. 1.2 which demonstrates flow over a heated flat plate. The plate temperature is T_w and the fluid free stream temperature and x-velocity component are T_∞ and u_∞, respectively. As the fluid comes into contact with the static plate, the fluid layer in the immediate vicinity of the plate comes to rest due to nonslip boundary condition. The particles in the adjoining fluid layer are
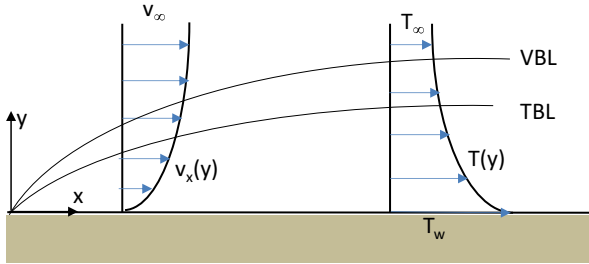
■ **FIGURE 1.2** Schematic showing the velocity and thermal boundary layer during convective heat transfer for flow over a flat plate.

then retarded due to the static layer. This retardation effect of fluid particles becomes weaker further away from the static plate in the y-direction until u approaches u_∞. The region of the fluid where u increases from 0 to u_∞ is called the velocity boundary layer denoted by VBL in Fig. 1.2. Similar to the VBL there exists a thermal boundary layer, TBL indicated in Fig. 1.2, where $T(y)$ decreases from T_w to T_∞. It is assumed here that $T_w > T_\infty$. If $T_w < T_\infty$ as in the case when the plate is heated by a flowing fluid, the temperature profile would be different with the fluid temperature, $T(y)$ increasing from T_w to T_∞. The thickness of both TBL and VBL gradually grow over the surface in the x-direction. The heat that is conducted into the fluid layer is transferred to the fluid outside the boundary layer. The heat flux between the solid plate and the fluid is given by applying Fourier's law to the fluid at the boundary [1],

$$q_w'' = -\kappa_f \frac{\partial T}{\partial y}\bigg|_{y=0} \tag{1.5}$$

where κ_f is the thermal conductivity of fluid. The heat transferred to the bulk of the fluid is then given by Newton's law of cooling which states that the heat flux is proportional to the temperature difference between the bulk and that at the surface of the plate [1],

$$q_w'' = h(T_w - T_\infty) \tag{1.6}$$

where h is the convective heat transfer coefficient. From Eqs. (1.5) and (1.6),

$$h = -\frac{\kappa_f}{(T_w - T_\infty)} \frac{\partial T}{\partial y}\bigg|_{y=0} \tag{1.7}$$

The heat transfer coefficient is a function of the length of the plate but in general the average heat transfer coefficient is used to calculate the heat flux. The convective heat transfer coefficient is related to the thermal conductivity by Nusselt number given by [1]

$$Nu_L = \frac{h_L L}{\kappa_f} \tag{1.8}$$

The Nusselt number is related to the fluid flow by Reynolds and Prandtl number. For laminar flow the correlation between Nusselt number and Reynolds and Prandtl numbers is given by [1]

$$Nu_{\mathrm{L}} = 0.664 \, Re_{\mathrm{L}}^{0.5} \, Pr_{\mathrm{L}}^{0.33} \tag{1.9}$$

for $Pr < 0.6$ and $Re_{\mathrm{L}} < 5 \times 10^5$. Convective heat transfer can be classified according to the nature of flow. If the flow is caused by external means like a blower or fan then the heat transfer is called forced convection. Forced convection can again be classified into the nature of flow, internal flow for flow through pipes or external flow such as flow external to surfaces as is shown in Fig. 1.2. If the flow is generated by buoyancy forces which arise due to difference in densities caused by temperature differential then the resultant mode of convective heat transfer is called natural convection. A good example of natural convection is the cooling of electronics inside a handheld device where there is no fan to force the flow.

1.1.3 **Radiation**

Along with conduction and convection, radiation heat transfer is another fundamental mode of heat transfer. Compared to other two modes, radiation can happen with and without any intervening medium. Also, unlike conduction and convection, radiation is not proportional to temperature gradient. Radiative heat transfer is dependent on the wavelength of thermal emission and the material properties of the bodies participating in the heat transfer are wavelength-dependent, unlike the other modes of heat transfer. While discussing radiation heat transfer some of the salient macroscale concepts will be discussed next. For further in-depth understanding of radiative heat transfer, interested readers should refer to the textbooks by Modest [3] and Siegel and Howell [4].

1.1.3.1 Blackbody Radiation

A blackbody is an ideal surface with the following properties.

1. Blackbody radiation absorbs all the incident radiation independent of wavelength and direction.
2. For a given wavelength and temperature, no surface can emit more energy than a blackbody.

Planck's distribution of blackbody radiation is given by [4]

$$I_{\lambda,\mathrm{b}}(\lambda, T) = \frac{2\mathrm{h}c^2}{\lambda^5 \left[e^{\frac{\mathrm{h}c}{k_{\mathrm{B}}\lambda T}} - 1 \right]} \tag{1.10}$$

where $I_{\lambda,b}$ is the blackbody intensity, $h = 6.6252 \times 10^{-34}$ J s, k_B is Boltzmann constant $= 1.38 \times 10^{-23}$ J/K, and c is the speed of light. The blackbody emissive power is given by $e_{b,\lambda}(\lambda,T) = \pi I_{b,\lambda}(\lambda,T)$. Integration of the blackbody emissive over the entire spectrum gives the famous Stefan–Boltzmann law, $e_b = \sigma T^4$. σ is the Stefan–Boltzmann constant whose value is 5.67×10^{-8} W/(m^2 K^4) and the unit of temperature is Kelvin. The wavelength, λ_{max} at which Planck's distribution reaches a maximum is given by [4]

$$\lambda_{max} = \frac{2898 \ \mu m \ K}{T[K]} \qquad (1.11)$$

Eq. (1.11) is also called Wien's displacement law, which links the maximum wavelength of thermal emission and temperature of medium.

Concept of blackbody radiation is purely from geometric optics or ray tracing. Using the concept of blackbody the emissivity of any surface can be defined as the ratio of radiation emitted by a surface to the radiation emitted by a blackbody at the same temperature. Radiative energy transfer between two media can be calculated by using either view factor [1] or classical radiative transfer equation for participating media which accounts for scattering, absorption, and transmission. Consider two flat plates with emissivities given by ε_1 and ε_2 at temperatures T_1 and T_2, respectively, as shown in Fig. 1.3, with $T_1 > T_2$. The plates are separated by an air gap and the distance between the plates is given by d. For the time being let us consider d to be greater than the peak wavelength (λ_T). From Wien's law, $\lambda_T = 2898/T_1$. The effect of d on the radiative heat transfer will be considered later in this chapter. Using ray tracing the radiative heat flux (q'') between the two plates shown in Fig. 1.3 is given by

$$q'' = \frac{\sigma\left(T_1^4 - T_2^4\right)}{\dfrac{1}{\varepsilon_1} + \dfrac{1}{\varepsilon_2} - 1} \qquad (1.12)$$
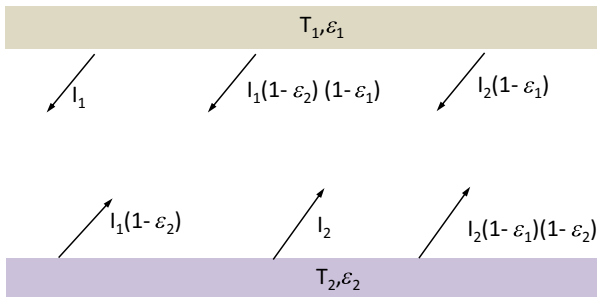
■ FIGURE 1.3 Schematic of radiative heat transfer between two plane surfaces separated by a distance d greater than the wavelength of thermal emission. The two walls are at temperatures T_1 and T_2 respectively and their emissivities are given by ε_1 and ε_2 respectively.

If both the surfaces are blackbodies, $\varepsilon_1 = \varepsilon_2 = 1$, $q'' = \sigma(T_1^4 - T_2^4)$. Max Planck in his book titled "The Theory of Heat Radiation" [5], while discussing the concept of blackbody, clearly mentioned that an inherent assumption of Planck's law is that "the linear dimensions of all the parts of space considered are large compared with the wavelength of the rays." Hence the concept of blackbody radiation is valid only when the bodies participating in radiation heat transfer and the distance separating them is larger than the wavelength of thermal radiation, as in Fig. 1.3. As the distance decreases and becomes comparable with or shorter than λ_{T}, near-field effects become important and ray optics can no longer be used to obtain the energy transfer between the two bodies. When the distance is on the order of nanometers the heat transfer is in the realms of near-field radiation. Before discussing near-field heat transfer let us investigate the entropy flow and generation in radiative heat transfer between surfaces when near-field effects are not considered. Entropy generation during radiation heat transfer has not been discussed in detail in any of the classical textbooks of radiation heat transfer so the following section should be extremely beneficial for the research community. Zhang and Basu [6] were the first to provide accurate expressions for entropy generation during radiation heat transfer as discussed in the next section.

1.2 ENTROPY FLOW AND GENERATION IN RADIATIVE TRANSFER BETWEEN SURFACES

The concept of entropy of radiation has played an essential role in the development of the theory of blackbody radiation. Boltzmann in 1884 investigated the thermodynamics of radiation in an isothermal enclosure and proved the empirical equation $e_{\mathrm{b}}(T) = \sigma T^4$ obtained by Stefan for the blackbody emissive power. Here, T is the temperature of the blackbody and σ is the Stefan−Boltzmann constant. In doing so, he also determined the associated entropy flux to be $s_{\mathrm{b}}(T) = 4/3\sigma T^3$. After introducing the radiation quanta, Planck expressed the spectral entropy associated with each vibrational frequency mode and formulated the famous law of blackbody radiation in 1900 [7]. Beretta and Gyftopoulos [6] pointed out that electromagnetic radiation carries both energy and entropy and is neither work nor heat interaction. In other words, for blackbody radiative transfer between two systems at different temperatures, the rate of entropy transfer is not equal to the ratio of energy transfer rate between the two systems to the temperature of either of the systems. Modeling a laser beam as an incoherent source and using the definition of spectral radiation entropy, Essex et al. [8] calculated the temperature of the near monochromatic laser radiation from a 1 mW He-Ne laser at 632.8 nm wavelength to be as high as

10^{10} K. Laser energy is considered as (almost) equivalent to work with very low entropy and a very high radiation temperature.

Petela [9] realized the importance of entropy and exergy of radiation to energy conversion in the 1960s. While the spectral nature of thermal radiation was recognized, he introduced a simplified formula, without spectral integration, for the total entropy leaving a diffuse-gray surface as $\varepsilon s_b(T_1)$, where ε is the emissivity and T_1 is the temperature of the emitting surface. Even for a free emitting surface, such an expression may result in a large error when the emissivity is small. In one of his recent papers on this subject, Petela [10] further assumed that the absorbed entropy of such a surface for radiation coming from a blackbody at temperature T_2 to be $\varepsilon s_b(T_2)$, which is also an oversimplification. In the 1980s, extensive studies were published to determine the maximum efficiency of solar energy converters [11−13]. These studies generally dealt with blackbody radiation and did not concern the spectral properties of radiation; see Bejan's text for a comprehensive review and discussion of this subject [13]. Arpaci [14] modeled radiation entropy generation for turbulent flow and heat transfer. His analysis was limited to optically thick cases when the radiative transfer equation is reduced to a diffusion equation similar to heat conduction.

Landsberg and Tongue [15] introduced the concept of *dilute blackbody radiation* and an *effective temperature*. They also proposed other temperature-related definitions such as the *flux temperature*, in addition to the *brightness temperature* [16]. However, they did not apply their theory for multiple reflections. Furthermore, the repeated usage of various definitions of temperature is confusing and prevents the general acceptance of their methodology. Wright et al. [17] obtained approximate expressions for calculating the entropy of radiation emitted from a gray body without considering reflection. Whale [18] drew an analogy between far-field radiation and near-field radiation using the concept of flux temperature but further research is needed to assess the validity of simply extending the far-field theory to the near-field situation. Caldas and Semiao [19] extended the formulation of radiation entropy to participating media and numerically determined the entropy generation during radiative transfer. However, the entropy generation at the wall that could be important for their studied systems was not included in their analysis and numerical simulation. Similar analysis was performed by Liu and Chu [20] considering a participating medium between blackbody walls.

In this section, attention is paid to the entropy associated with the emission, transmission, and reflection processes of thermal radiation by a surface, which is opaque or semi-infinite, or a semitransparent slab. Furthermore,

the entropy generation during radiative transfer between two isothermal diffuse-gray surfaces is analyzed, considering the entropy components associated with absorption, emission, and reflection of radiation. The entire analysis has been performed without considering interference and photon tunneling. Second law analysis of near-field radiation will be discussed in Section 1.4.

For a blackbody enclosure at thermal equilibrium, one can use a cylinder-piston arrangement to perform a thermodynamic analysis that will lead to the Stefan–Boltzmann law, and expressions for the entropy, pressure, and specific heat of blackbody radiation in terms of its temperature [3,4]. For blackbody radiation in vacuum, the spectral distributions of the emissive power and intensity are given by Planck's law,

$$e_{\lambda,b}(\lambda, T) = \pi I_{\lambda,b}(\lambda, T) = \frac{\beta \pi h c^2}{\lambda^5 (e^{hc/k_B \lambda T} - 1)} \tag{1.13}$$

where c is speed of light in vacuum, h is Planck's constant, and k_B is Boltzmann's constant. Here, β is a polarization parameter in such a way that $\beta = 1$ is for either the transverse electric (TE) wave or the transverse magnetic (TM) wave, and $\beta = 2$ is for unpolarized radiation. It is noticed that the intensity of blackbody radiation is independent of direction. The *radiation entropy intensity* can be expressed in terms of the (energy) intensity as follows [5].

$$L_\lambda(I_\lambda) = \frac{\beta k_B c}{\lambda^4} \left[\left(1 + \frac{\lambda^5 I_\lambda}{\beta h c^2}\right) \ln\left(1 + \frac{\lambda^5 I_\lambda}{\beta h c^2}\right) - \frac{\lambda^5 I_\lambda}{\beta h c^2} \ln\left(\frac{\lambda^5 I_\lambda}{\beta h c^2}\right) \right] \tag{1.14}$$

The radiation entropy flux is calculated by integrating the radiation entropy intensity, that is,

$$s_\lambda = \int_{\theta=0}^{\pi} \int_{\phi=0}^{\pi/2} L_\lambda \cos\theta \sin\theta \, d\theta d\phi \tag{1.15}$$

For a blackbody or diffuse radiation, we have $s_\lambda = \pi L_\lambda$. In a closed enclosure with a volume V, the temperature of the system is defined as $\frac{1}{T} = \left(\frac{\partial S}{\partial U}\right)_V$, where S and U refer to the entropy and internal energy of the system, respectively [6]. The *monochromatic radiation temperature*, or simply either the *monochromatic temperature* or *radiation temperature*, can be defined based on the spectral intensities (since they are proportional to the energy and entropy densities of the electromagnetic radiation), namely

$$\frac{1}{T_\lambda(\lambda, \Omega)} = \frac{\partial L_\lambda}{\partial I_\lambda} \tag{1.16}$$

At thermodynamic equilibrium, it is obvious that the above expression gives the physical temperature of the photon gas regardless of the radiative properties of the wall, as long as the location is not too close to the surface of the wall where near-field radiation dominates. One can rewrite Eq. (1.16) using Eq. (1.14) as follows:

$$T_\lambda(I_\lambda) = \frac{hc/\lambda k_B}{\ln\left(\dfrac{\beta hc^2}{\lambda^5 I_\lambda} + 1\right)} \tag{1.17}$$

Considering a nearly monochromatic laser beam from a pointer, the intensity I_λ can easily be calculated based on its power, wavelength interval, beam diameter, and divergence. Assuming that the light is polarized and can be treated as in an equilibrium state, the entropy intensity L_λ can be calculated from Eq. (1.14) and, similarly, the "temperature" of the laser light can be obtained by either Eq. (1.16) or Eq. (1.17). It can be easily shown that this temperature is the one that corresponds to a blackbody radiation spectrum with the same intensity at the laser wavelength. Such a temperature is often called the brightness temperature or *radiance temperature*, in optical pyrometry and radiation thermometry [21] as an equivalent temperature that a blackbody would have in order for it to emit the same intensity. The entropy defined in Eq. (1.14) is generally applicable for incoherent radiation, as can be proved by nonequilibrium thermodynamics [6]. Furthermore, the temperature defined in Eq. (1.16) is a thermodynamic temperature for the monochromatic or spectral-directional radiation [16]. As pointed out by Caldas and Semiao [19], there exist *infinite* radiation temperatures at any spatial location for steady-state thermal radiation in an enclosure that is not at thermal equilibrium. An immediate paradox is as follows. If a surface, whose emissivity is not equal to 1, is placed inside a blackbody enclosure, what is the temperature of the emitted, reflected, and absorbed radiation? The solution is that one should substitute the *combined intensity*, rather than the reflected intensity or emitted intensity, into Eq. (1.14) to evaluate the entropy and into Eq. (1.17) to evaluate the temperature. Because the enclosure is at thermal equilibrium, the combined intensity is independent of the surface properties and wavelength. The obtained monochromatic temperature based on the combined intensity will always be the equilibrium temperature of the enclosure. Multiple reflections can be treated in the same way by using their combined intensity to define the radiation temperature. Entropy production can occur in radiation without the generation of heat. If a nearly collimated radiation is diffusely scattered by a perfectly reflecting (rough) surface, the scattered radiation will have a much lower intensity due to the expanded solid angle. The process is accompanied by entropy increase and hence is irreversible. On the other hand, if a nearly collimated light is

split into two beams using a beamsplitter, the transmitted and reflected beams can interfere with each other and the original intensity can be realized again after another beamsplitter in the Mach−Zehnder interferometer. This process may be reversible because the two beams are correlated [22]. The correlated or coherent beams have lower entropy than those with the same intensity at thermodynamic equilibrium. The concept of monochromatic temperature is applicable only if the maximum entropy has been obtained. The calculation of radiation entropy based on Eq. (1.14) relies on the following three hypotheses.

1. For either a vacuum or a participating medium, the intensities of radiation at any given location can be superimposed regardless of where they originate, as long as all the rays fall within the same infinitesimal solid angle (pencil cone) and spectral interval (either based on the wavelength or frequency). The resulting intensity is called the combined intensity. Note that the intensity cannot be a simple addition in the presence of strong interference and diffraction. In essence, wave interference and diffraction effects are neglected, and the radiation field is treated as incoherent under this hypothesis. Furthermore, if a participating medium is present, it is assumed nondispersive so that the group velocity and the phase velocity of electromagnetic waves are the same and independent of the frequency.

2. The monochromatic radiation temperature can be calculated based on Eq. (1.17) using the combined intensity. Radiation temperature is in general dependent on the wavelength or frequency, direction, and polarization. Photons are relativistic quanta that behave very differently from molecules or electrons. Photons travel with the same speed and do not collide with each other. The interaction between photons is a wave effect that has been excluded in the first hypothesis. Hence, photons of different frequencies can coexist in the same volume element but with different radiation temperatures. In addition, photons in different directions can have different monochromatic temperatures even with the same frequency. In the case when the radiation consists of two linear polarizations with different intensities, the monochromatic temperatures will be different for different polarizations. In essence, nonequilibrium radiation may be regarded as in a partial equilibrium state, so that each subsystem with its own wavelength, direction, and polarization can be considered as in an equilibrium state that is independent of others. A detailed discussion about partial thermodynamic equilibrium can be found in Ref. [23]. It should also be noted that if the medium is optically thick, local equilibrium will be established; in which case the radiation temperature reduces to the local temperature of the medium.

3. The entropy intensity is defined based on the combined intensity according to Eq. (1.14). The sum of the entropies of all individual rays should be calculated based on the radiation temperature of the combined intensity. Because both energy and entropy are additive, the ratio of the entropy intensity of each ray to the entropy intensity of the combined radiation is equal to the ratio of the (energy) intensity of that ray to the combined intensity. This hypothesis allows evaluation of the absorbed, emitted, and reflected entropy at individual surfaces.

The logical interpretation of radiation temperature and radiation entropy allows a thermodynamic analysis of radiative heat transfer in various situations. The present study focuses on the radiative transfer between surfaces. The energy and entropy equations for a plate at temperature T_1 whose surface emissivity is ε_1 can be derived with the help of Fig. 1.4. The elemental solid angle is $d\Omega$, and its direction is indicated by Ω, which is determined by the zenith angle θ from surface normal $\hat{\mathbf{n}}$ and the azimuthal angle ϕ. It is assumed that radiation is absorbed or emitted from a very thin skin layer.

The energy balance of the control volume per unit surface area can be written as

$$\dot{U} = q_{\text{in}} - q_{\text{out}} + q_{\text{cond}} \tag{1.18}$$

where $\dot{U}$ is the rate of internal energy change in the control volume, q_{in} and q_{out} are the incoming and outgoing radiative heat flux (or energy flux to be
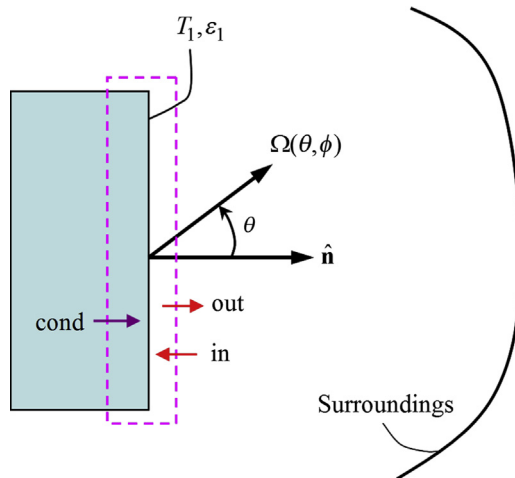
■ **FIGURE 1.4** Energy and entropy balance for radiative heat transfer at the surface of a plate. *With permission from Zhang ZM, Basu S. Entropy flow and generation in radiative transfer between surfaces. Int J Heat Mass Transfer 2007;50:702—12, Figure 1.*

more precise), and q_{cond} is the conduction heat flux entering the left side of the control volume. Hemispherical and spectral integration of the intensity gives the heat fluxes:

$$q_{in} = \int_{\lambda=0}^{\infty} d\lambda \int_{\widehat{\mathbf{n}}\cdot\Omega<0} I_{\lambda}(\lambda,\Omega)\widehat{\mathbf{n}}\cdot\Omega \, d\Omega \qquad (1.19a)$$

and

$$q_{out} = \int_{\lambda=0}^{\infty} d\lambda \int_{\widehat{\mathbf{n}}\cdot\Omega>0} I_{\lambda}(\lambda,\Omega)\widehat{\mathbf{n}}\cdot\Omega \, d\Omega \qquad (1.19b)$$

For the outgoing radiation, the intensity is the sum of the emitted and the reflected intensities. These equations have been studied extensively in radiative transfer texts [3,4] and will not be repeated here. The next step is to express the entropy balance as follows [13,23]:

$$\dot{S} = s_{in} - s_{out} + s_{cond} + s_g \qquad (1.20)$$

All quantities expressed above are for unit time and unit area, and the subscripts have the same meaning as in Eq. (1.18), except that g stands for generation. Eq. (1.20) states that the change of entropy in the control volume is equal to the net entropy received by the control volume plus entropy generation. Similar to the heat fluxes, the entropy fluxes can be calculated by

$$s_{in} = \int_{0}^{\infty} d\lambda \int_{\widehat{\mathbf{n}}\cdot\Omega<0} L_{\lambda}(\lambda,\Omega)\widehat{\mathbf{n}}\cdot\Omega \, d\Omega \qquad (1.21a)$$

and

$$s_{out} = \int_{0}^{\infty} d\lambda \int_{\widehat{\mathbf{n}}\cdot\Omega>0} L_{\lambda}(\lambda,\Omega)\widehat{\mathbf{n}}\cdot\Omega \, d\Omega \qquad (1.21b)$$

where L_{λ} is determined from I_{λ} by Eq. (1.14). Because the plate is maintained at a constant temperature, assuming the thermal conductivity is very high, $s_{cond} = q_{cond}/T_1$. The left-hand sides in Eqs. (1.18) and (1.20) are zero at the steady state. Therefore, Eq. (1.21) can be recast to evaluate the entropy generation rate per unit surface areas due to radiative heat transfer in the following.

$$s_g = \frac{q_{in} - q_{out}}{T_1} - (s_{in} - s_{out}) \qquad (1.22)$$

Similar to radiative heat transfer analysis [4], entropy flow toward a surface and away from a surface can be characterized by an incoming component and an outgoing component. Can one separate the emitted entropy from the reflected entropy? Yes. This can be done by first separating the outgoing

intensity into an emitted component, which is the emissivity multiplied by the blackbody emissive power, and a reflected component, which depends on the incident spectral intensity and the bidirectional reflectance of the surface. The ratio of the emitted intensity to the combined intensity is a function of the wavelength and direction, given by

$$X(\lambda, \Omega) = \varepsilon_1 I_{\lambda,\text{b}}(\lambda, T)/I_\lambda, \quad \text{for } \Omega \cdot \hat{\mathbf{n}} > 0 \text{ only} \tag{1.23}$$

where the function X is the fraction of the emitted intensity, and ε_1 in general is dependent on the wavelength and direction as well. The emitted entropy can be calculated by

$$L_{\lambda,\text{emit}}(\lambda, \Omega) = X(\lambda, \Omega)L_\lambda(I_\lambda) \tag{1.24}$$

Notice again that the combined entropy intensity L_λ is evaluated from the combined intensity I_λ by Eq. (1.14). The proportionality used in Eqs. (1.23) and (1.24) is based on the concept of partial equilibrium or spectral-directional equilibrium of thermal radiation as outlined in the second hypothesis given above. In an equilibrium state, if the number of particles is divided by two, the energy and entropy are also equally divided because both are extensive properties. The emitted entropy flux, s_{emit}, can be obtained by substituting $L_{\lambda,\text{emit}}(\lambda, \Omega)$ for $L_\lambda(\lambda, \Omega)$ into Eq. (1.21b) and then performing the integration. The reflected entropy flux becomes $s_{\text{ref}} = s_{\text{out}} - s_{\text{emit}}$, and the absorbed entropy flux is thus $s_{\text{abs}} = s_{\text{in}} - s_{\text{ref}} = s_{\text{in}} - s_{\text{out}} + s_{\text{emit}}$.

The physical interpretation of the entropy of emission is the entropy associated with the photons that are emitted by the surface (only spontaneous emission is considered here). The radiative energy emitted by the surface depends only on its temperature and emissivity, independent of the environment. On the contrary, the emitted entropy is dependent on the incoming radiation, if the incoming radiation from the surrounding cannot be neglected. The reason is that the monochromatic temperature of emission is affected by the incoming photons. For the same amount of photon flux, the entropy of free emission, ie, $X(\lambda, \Omega) = 1$, is different from the entropy of emission when the incoming intensity is nonzero.

1.2.1 **Entropy Analysis Applied to Special Cases**

Several special cases are chosen to illustrate the entropy formulation in radiative heat transfer. The first case is for *free emission* from a diffuse-gray body. Here, free emission means that the surface is enclosed in an empty space with large surroundings at zero absolute temperature. The second case is for free emission from a semi-infinite medium with a refractive index that is independent of wavelength. Therefore, the surface is gray but

not diffuse and there is an effect of polarization on the emission. The third case is the entropy generated upon reflection and transmission through a semitransparent slab of given refractive index. The effects of polarization and multiple reflections are considered, but interference and absorption are neglected. Semitransparent windows are extensively used in solar energy applications, including in solar collectors and buildings. The fourth case is the radiative transfer between two infinite parallel plates at different temperatures separated by vacuum. Both the plates are modeled as diffuse-gray and opaque with different emissivities. The separation distance is assumed to be large enough so that interference and evanescent wave effects can be neglected. At steady state, partial radiation equilibrium is established inside such a cavity but the radiation temperature depends on both the wavelength and direction. The entropy generation due to the emission, reflection, and absorption of thermal radiation is analyzed for each surface.

1.2.1.1 Free Emission From a Diffuse-Gray Surface

The simplest case besides blackbody emission is a diffuse-gray surface emitting toward a large, cold environment. There is no absorption and no incoming fluxes, and from the definition of emissivity, the outgoing or emitted heat flux is

$$q_{\text{emit}} = \varepsilon \sigma T^4 \tag{1.25}$$

where ε and T are the emissivity and temperature of the surface (the subscript 1 in Fig. 1.4) is omitted for simplicity). Intuitively, one would guess that, in analogy to the blackbody emission with an emissive power $e_b = \sigma T^4$ and entropy flux of $s_b = 4/3\sigma T^3$, the total emitted entropy flux of the diffuse-gray surface could be given by

$$s_{\text{emit}} = \varepsilon \frac{4}{3} \sigma T^3 \tag{1.26}$$

This is Eq. (7) in the 1964 paper by Petela [9]. After some 40 years, the same equation was used in his 2003 paper for gray surfaces, see Eq. (29) in Ref. [10]. If Eq. (1.26) holds, the entropy generation by free emission becomes

$$s_g = s_{\text{emit}} - \frac{q_{\text{emit}}}{T} = \frac{1}{3} \varepsilon \sigma T^3 \tag{1.27}$$

which is Eq. (30) in Ref. [10]. Fig. 1.5 shows the calculation results according to Eq. (1.9b), which is called the exact solution, and Petela's approximate expression, ie, Eq. (1.26) in this chapter. The emitted entropy is normalized to the blackbody entropy. It can be seen from Fig. 1.5 that Eq. (1.26) is exact
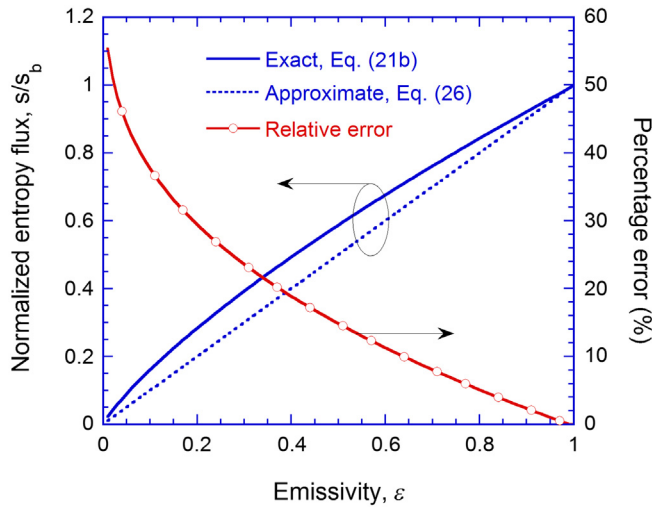
■ **FIGURE 1.5** Outgoing entropy flux, normalized to that of a blackbody, for a free emitting surface as a function of its emissivity. The percentage error of the approximation is shown on the right. *With permission from Zhang ZM, Basu S. Entropy flow and generation in radiative transfer between surfaces. Int J Heat Mass Transfer 2007;50:702—12, Figure 2.*

only when the emissivity is equal to 1, as for the blackbody case. When the emissivity is less than unity, Eq. (1.26) always underpredicts the emitted entropy, and hence the entropy generation according to Eq. (1.27) is also erroneously underpredicted. The error caused by this approximation may be small if the source has a large emissivity value or is near a blackbody. Nevertheless, caution should be taken before applying Eq. (1.26) in analyzing the conversion efficiencies for nonideal surfaces. The reason why the total emissivity should not be directly used in the total entropy expression is the following. Consider a source temperature at 3000 K, the blackbody emissive power is the highest as shown in Fig. 1.6A. For a diffuse-gray surface with an emissivity of 0.5, the spectral distribution of the emissive power would be proportional to the blackbody emissive power at 3000 K. This curve, however, is not a blackbody distribution function. Suppose an equivalent temperature of the radiation based on the total emissive power is to be used. By setting $\sigma T'^4 = \varepsilon \sigma T^4$, one obtains $T' = 1681.8$ K. The peak of the spectral distribution that corresponds to the blackbody distribution at T' will shift to a longer wavelength, as illustrated in Fig. 1.6A. Only at the crossover wavelength, which is approximately 1.33 μm, is the monochromatic temperature of the diffuse-gray body the same as T'. In other words, the radiation temperature even for a gray body is wavelength-dependent. The nonequilibrium nature of gray-surface emission was noticed by Landsberg and Tonge
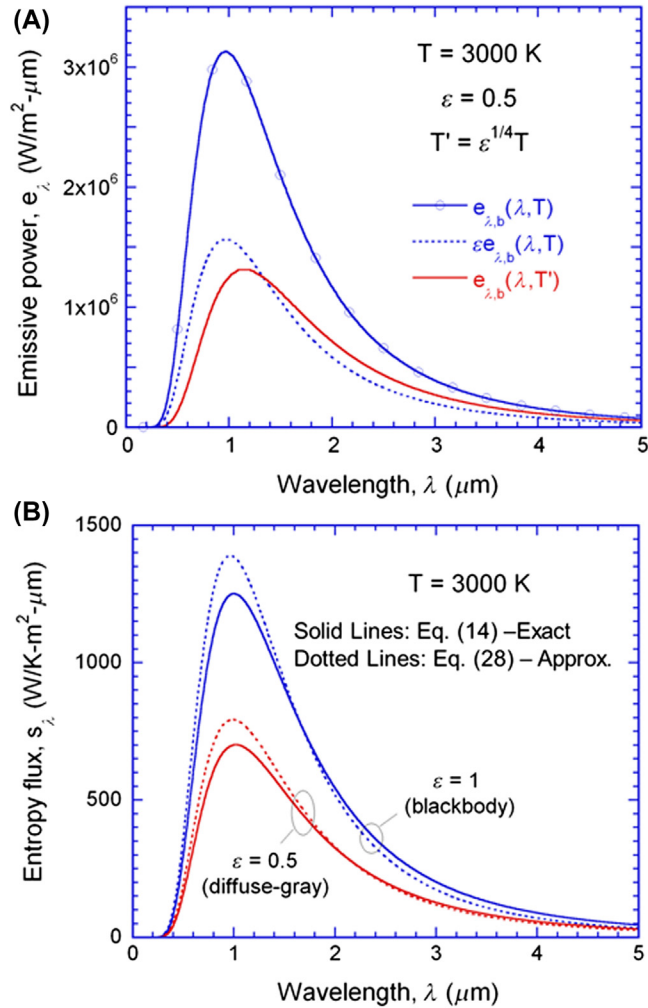
■ FIGURE 1.6 Spectral distribution of (A) emissive power and (B) entropy flux. *With permission from Zhang ZM, Basu S. Entropy flow and generation in radiative transfer between surfaces. Int J Heat Mass Transfer 2007;50:702—12, Figure 3.*

[14] who called this type of radiation as dilute blackbody radiation. In the present discussion only very few new definitions are used, and the entropy analysis is directly to linked thermal radiation analysis for which the heat transfer community is already very familiar with.

Bejan arrived at an expression for the radiation entropy intensity:

$$L_\lambda = \frac{4I_\lambda}{3T_\lambda} \tag{1.28}$$

which is Eq. (9.47) in Ref. [13]. For radiation from a blackbody, the mono-chromatic temperature is not a function of wavelength; hence, the spectral integration of Eq. (1.28) yields $L = 4/3 \; \frac{\sigma T^3}{\pi}$, as expected. A direct compar-ison of the spectral distribution between the exact expression of L_λ given in Eq. (1.14) and the approximate expression of Eq. (1.28) is shown in Fig. 1.6B. It can be seen that the approximate expression overpredicts the entropy flux at shorter wavelengths and underpredicts the entropy flux at longer wavelengths, even for a blackbody source. Given the available computational capabilities nowadays, it is a relatively easy task to perform the integration using the spectral entropy distribution given in Eqn (1.14) to prevent the error associated with this approximation.

The radiation temperature is plotted against wavelength for diffuse-gray sur-faces with different emissivities, as shown in Fig. 1.7. The radiation temper-ature is the same as the surface temperature for a blackbody and is independent of wavelength. As the emissivity is reduced, the monochro-matic temperature decreases faster at longer wavelengths, ie, in the Rayleigh—Jeans limit, where the blackbody emissive power is proportional to temperature. At very short wavelengths, the emissive power is a strong function of temperature, and thus the effect of emissivity on the radiation temperature is very weak.

■ **FIGURE 1.7** Spectral distribution of the monochromatic temperature for free emitting surfaces at 3000 K with different emissivities. *With permission from Zhang ZM, Basu S. Entropy flow and generation in radiative transfer between surfaces. Int J Heat Mass Transfer 2007;50:702—12, Figure 4.*
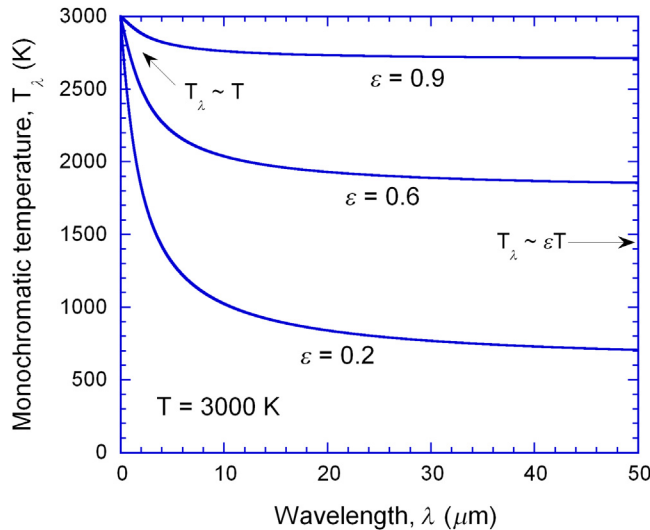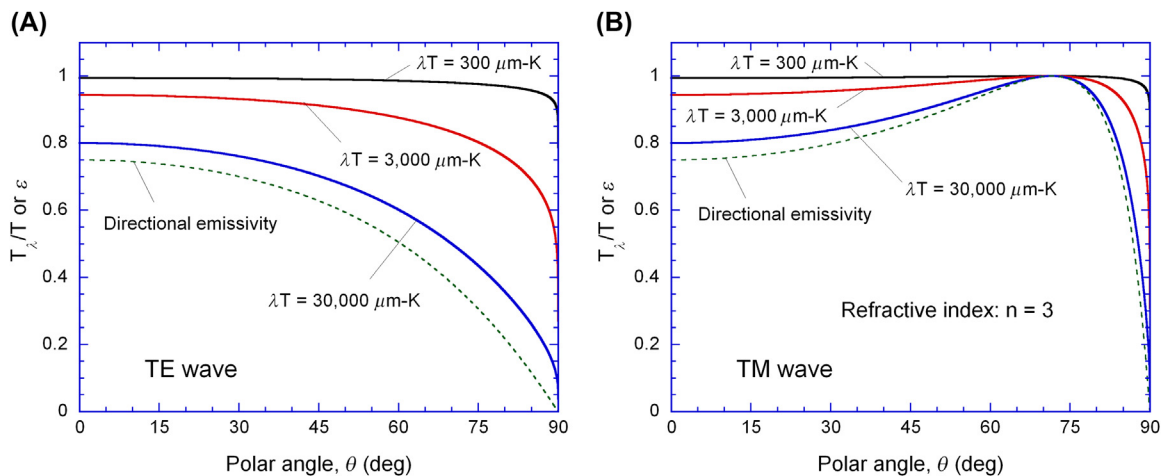
1.2.1.2 Free Emission From a Semi-infinite Medium With Refractive Index n

For the purpose of illustrating the polarization effect, a semi-infinite medium with a refractive index n at a uniform temperature T is considered as the emission source. The emission is again toward free space. The emissivity for either TE or TM wave can be calculated based on Kirchhoff's law by subtracting the reflectivity calculated using Fresnel's equations [21]. The emitted intensity for each polarization is used to compute the entropy of emission and monochromatic temperature. The ratio of the monochromatic temperature to the medium temperature is shown in Fig. 1.8, along with the directional emissivity, for $n = 3$ for both polarizations. Note that the temperature ratio depends on the product λT and $\lambda T = 3000 \ \mu$m K is near the peak wavelength in the emissive power given by Wien's displacement law and 99.5% of the radiative energy is within the spectral region from $\lambda T = 300 \ \mu$m K to $\lambda T = 30,000 \ \mu$m K. At the Brewster angle ($\theta_B = 71.57$ degree), where the emissivity is equal to 1, the monochromatic temperature is the same as the temperature of the medium. The effect of angular dependence and polarization is clearly demonstrated in Fig. 1.8. Note again that the effect of emissivity on the monochromatic temperature is larger toward longer wavelengths.

The normalized emitted entropy as a function of the refractive index is shown in Fig. 1.9, together with the hemispherical and normal emissivities.

■ **FIGURE 1.8** Temperature ratio versus the polar angle for thermal emission from a semi-infinite medium with a refractive index $n = 3$, where the directional emissivity is also shown. (A) TE wave; (B) TM wave. *With permission from Zhang ZM, Basu S. Entropy flow and generation in radiative transfer between surfaces. Int J Heat Mass Transfer 2007;50:702—12, Figure 5.*
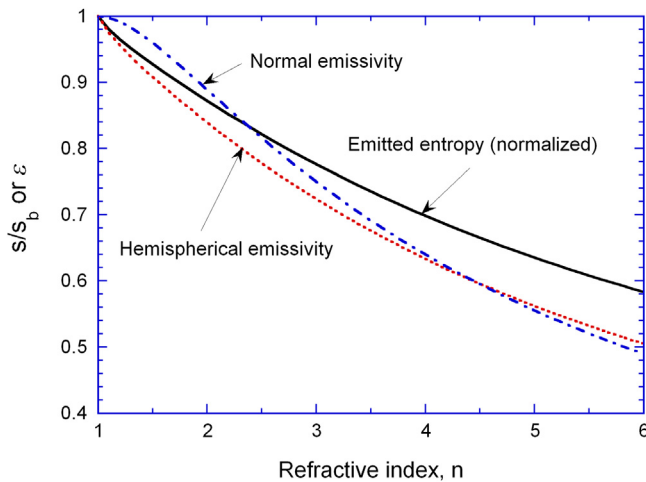
■ **FIGURE 1.9** Emitted entropy flux, normalized to that of a blackbody at the same temperature, hemispherical emissivity, and normal emissivity versus the refractive index of the emitting medium. *With permission from Zhang ZM, Basu S. Entropy flow and generation in radiative transfer between surfaces. Int J Heat Mass Transfer 2007;50:702—12, Figure 6.*

Note that a constant refractive index is assumed so that the emission is independent of the wavelength. For a gray surface, $s/s_b \neq f(T)$ as can be seen from Eqs. (1.14) and (1.21b). The hemispherical emissivity is obtained by integrating the average emissivity over the hemisphere. For the entropy calculation, individual emissivity is first multiplied by the blackbody intensity to evaluate the entropy intensity. The entropy intensity is then integrated over the hemisphere and wavelength and then the two polarization components are added. While the surface is not diffuse, it is interesting to see how much error it would cause in the entropy flux when the surface is assumed to be a diffuse surface with an emissivity equal to the hemispherical emissivity. Table 1.1 compares the entropy fluxes. Regardless of the large differences in

Table 1.1 Entropy Flux for a Free-Emitting Semi-infinite Medium

Refractive Index (n)	1	2	3	4	5	6
Hemispherical emissivity	1	0.839	0.724	0.633	0.562	0.505
s/s_b (exact solution)	1	0.872	0.776	0.698	0.635	0.583
s/s_b (diffuse assumption)	1	0.874	0.781	0.705	0.643	0.592
Relative error	0	0.2%	0.6%	1.0%	1.2%	1.5%

the monochromatic temperature of the emitted radiation, the diffuse assumption gives excellent prediction for the entropy flux, which is less than 1% when the emissivity is higher than 0.65 and only 1.5% when the emissivity is 0.5.

1.2.1.3 Reflection and Transmission of Solar Radiation by a Window

Attention is now turned to the case of entropy generation for solar radiation at a glass window. The typical refractive index of fused silica is $n = 1.5$, and absorption can be neglected in the most important solar spectrum from about 0.25 to 3.5 μm. The transmittance and reflectance can be calculated based on the ray-tracing method so that the transmitted and reflected intensities can be evaluated for each polarization as functions of the incidence polar angle [4]. The incident, reflected, and transmitted entropy intensities can be evaluated based on the spectral energy intensities. Because the radiation from the sun is confined in a small solid angle, it can be considered as a nearly collimated beam. In the calculation, the temperature of the sun is assumed to be $T_0 = 5800$ K. For illustration purposes, atmospheric absorption and scattering are neglected so that the intensity arriving at the window is taken to be the same as that of a blackbody at T_0. The sum of the reflected and transmitted entropy fluxes will be greater than the incidence entropy flux due to irreversibility. The difference is the entropy generation.

The nondimensionalized total and spectral entropy generation is shown in Fig. 1.10, where q_0 is the incident heat flux and is equal to the blackbody emissive power of the sun since scattering and absorption by the atmosphere is neglected. In reality, atmospheric effects will not only reduce the incoming intensity of the solar radiation but also its monochromatic temperature. The curves are plotted for both TE wave and TM wave. For TE wave, the reflectance increases as the incidence angle increases. At the glazing angle, all the incident radiation is reflected and the entropy generation becomes zero for both polarizations. For TM wave, the reflectance is first reduced until the Brewster angle, which is 56.3° with $n = 1.5$. At the Brewster angle, all incident radiation is transmitted and the entropy generation is zero. The peak entropy generation corresponds to the case when the incident power is split nearly equally into the transmitted and reflected beams. The angular dependence of the spectral entropy generation follows the same trend for corresponding polarization. However, the entropy generation normalized to the spectral intensity increases rapidly as the wavelength increases. Not surprisingly, the nondimensional total entropy generation is close to the spectral entropy generation at the wavelength (0.5 μm) close to the maximum wavelength of emission.
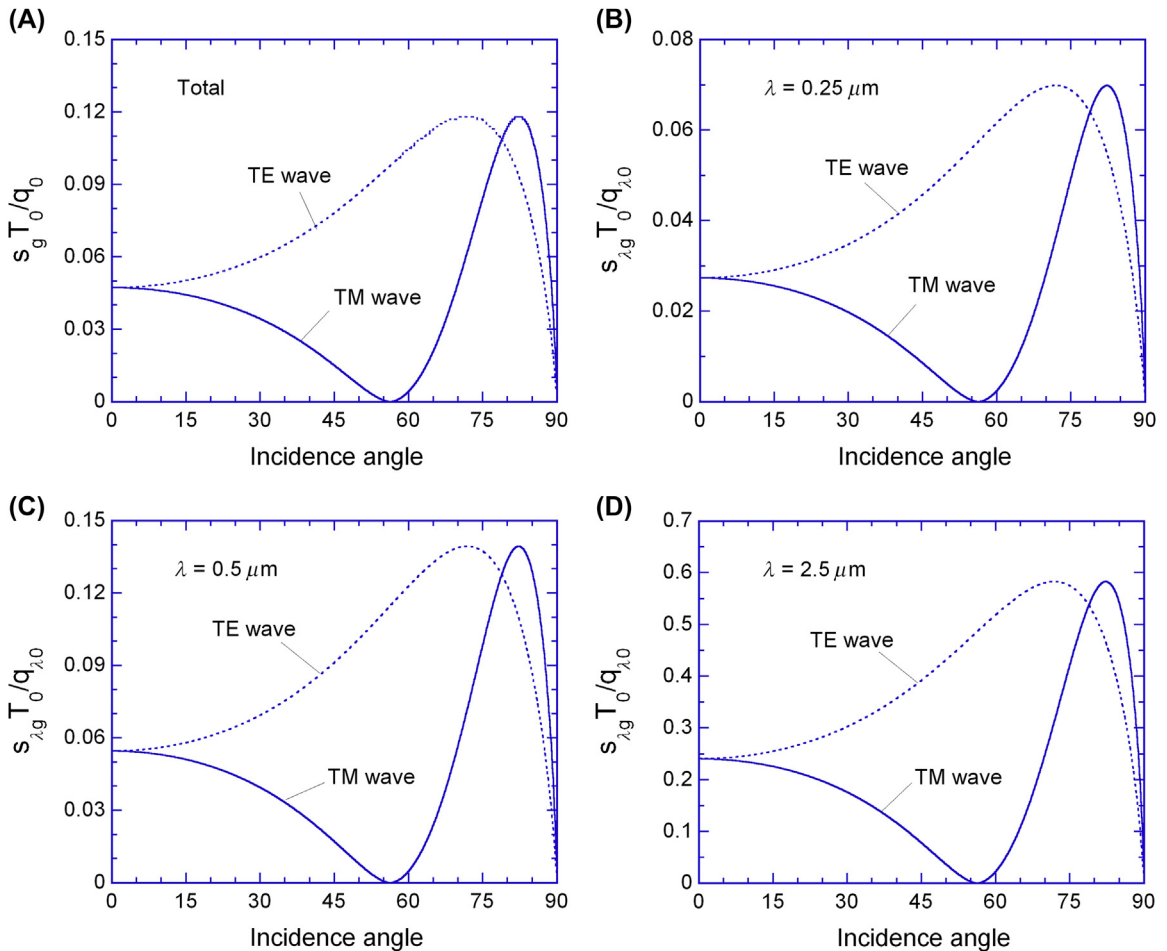
■ FIGURE 1.10 Total and spectral entropy generation of solar radiation upon reflection and transmission through a glass window, where T_0 is the temperature of the sun, $q_0 = \sigma T_0^4$, and $q_{\lambda 0} = e_{\lambda,b}(\lambda, T_0)$. *With permission from Zhang ZM, Basu S. Entropy flow and generation in radiative transfer between surfaces. Int J Heat Mass Transfer 2007;50:702—12, Figure 7.*

1.2.1.4 *Radiative Transfer Between Parallel Plates*

So far, the discussion about free emission, reflection, and transmission may be viewed as a natural extension of the more complicated thermodynamic models of photon radiation, as summarized by Landsberg and Tonge [16] in 1980. The final example is for two large parallel plates at temperatures T_1 and T_2, separated by vacuum, as shown in Fig. 1.11. For convenience of discussion without loss of generality, it is assumed that $T_1 \geq T_2$. The surfaces of the plates are assumed diffuse and gray with emissivities ε_1 and ε_2, respectively. The separation distance is sufficiently large so that the near-field effects can be neglected [24].

$$I_\lambda^+ = \varepsilon_1 I_{\lambda,b1} + \varepsilon_1 I_{\lambda,b1}(1-\varepsilon_1)(1-\varepsilon_2) + \dots$$
$$+ (1-\varepsilon_1)\varepsilon_2 I_{\lambda,b2} + (1-\varepsilon_1)\varepsilon_2 I_{\lambda,b2}(1-\varepsilon_1)(1-\varepsilon_2) + \dots$$
$$I_\lambda^- = (1-\varepsilon_2)\varepsilon_1 I_{\lambda,b1} + (1-\varepsilon_2)\varepsilon_1 I_{\lambda,b1}(1-\varepsilon_1)(1-\varepsilon_2) + \dots$$
$$+ \varepsilon_2 I_{\lambda,b2} + \varepsilon_2 I_{\lambda,b2}(1-\varepsilon_1)(1-\varepsilon_2) + \dots$$
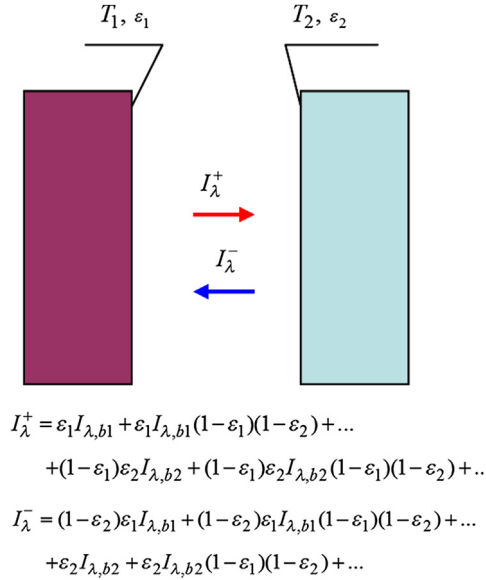
■ **FIGURE 1.11** Radiative heat transfer between two plates, showing the ray-tracing scheme for the forward and backward intensities, assuming $T_1 \geq T_2$. With permission from Zhang ZM, Basu S. Entropy flow and generation in radiative transfer between surfaces. Int J Heat Mass Transfer 2007;50:702—12, Figure 8.

The condition that both surfaces are diffuse and gray allows the determination of the forward intensity I_λ^+ and backward intensity I_λ^- as follows,

$$I_\lambda^+ = \frac{\varepsilon_1 I_{\lambda,b1} + (1-\varepsilon_1)\varepsilon_2 I_{\lambda,b2}}{1 - (1-\varepsilon_1)(1-\varepsilon_2)}$$

and

$$I_\lambda^- = \frac{\varepsilon_1(1-\varepsilon_2)I_{\lambda,b1} + \varepsilon_2 I_{\lambda,b2}}{1 - (1-\varepsilon_1)(1-\varepsilon_2)} \tag{1.29}$$

where $I_{\lambda,b1}$ and $I_{\lambda,b2}$ are Planck's distributions evaluated at T_1 and T_2, respectively. The radiation can be considered unpolarized because of the diffuse-gray assumption. Eq. (1.29) can be obtained using the ray-tracing method [4] as shown in Fig. 1.11. The forward and backward intensities can be substituted into Eq. (1.17) to calculate the monochromatic temperatures: T_λ^+ and T_λ^-, respectively, for the forward and backward radiation. In the special case when $\varepsilon_1 = 0$ but $\varepsilon_2 \neq 0, I_\lambda^+ = I_\lambda^- = I_{\lambda,b2}$. The photon gas will be in equilibrium with surface 2. On the other hand, if surface 2 is perfectly reflecting, then the photon gas will be in equilibrium with surface 1. When $\varepsilon_1 = \varepsilon_2 = 1$, ie, both surfaces are blackbodies, $T_\lambda^+ = T_1$ and $T_\lambda^- = T_2$, the forward stream and backward stream of photons can be viewed as being at different equilibrium states. In the extreme case when

$T_1 = T_2$, it can be seen from Eq. (1.17) that $I_\lambda^+ = I_\lambda^- = I_{\lambda,b1} = I_{\lambda,b2}$, suggesting that a complete or *stable equilibrium state* [23] will be established. When nonideal surfaces are involved, the monochromatic temperature will be wavelength-dependent, as can be seen from Fig. 1.12 for $T_1 = 1500$ K, $T_2 = 300$ K. In general $T_1 \geq T_\lambda^+ \geq T_\lambda^- \geq T_2$. In the case when $\varepsilon_2 = 0$, the monochromatic temperature is T_1. When $\varepsilon_1 = 0.2$ and $\varepsilon_2 = 1$, $T_\lambda^- = T_2$ but T_λ^+ is wavelength-dependent. When $\varepsilon_1 = \varepsilon_2 = 0.5$, both T_λ^+ and T_λ^- decrease toward longer wavelengths.

The strategy of computing the entropy is to evaluate the entropy intensities using Eq. (1.2) by substituting the forward and backward intensities calculated from Eq. (1.17). The results give L_λ^+ and L_λ^- that are independent of the polar angle. Hence, the entropy fluxes can be calculated by

$$s^+ = \pi \int_0^\infty L_\lambda^+ \, d\lambda \text{ and } s^- = \pi \int_0^\infty L_\lambda^- \, d\lambda \tag{1.30}$$

Note that for surface 1, the "+" sign is for the outgoing and the "−" sign is for the incoming, and the opposite is the case for surface 2. The entropy generation at each surface due to radiative heat transfer can thus be evaluated using Eq. (1.22). Let $q_{12} = q^+ - q^-$ and $s_{12} = s^+ - s^-$, which are the net heat transfer and entropy transfer, the entropy generation at each surface can be expressed as

$$s_{g,1} = s_{12} - \frac{q_{12}}{T_1} \geq 0 \text{ and } s_{g,2} = \frac{q_{12}}{T_2} - s_{12} \geq 0 \tag{1.31}$$
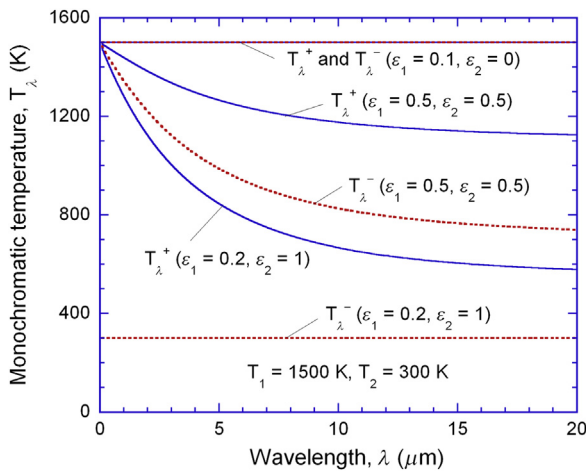

■ **FIGURE 1.12** Monochromatic temperature versus wavelength when $T_1 = 1500$ K and $T_2 = 300$ K with different emissivity combinations. *With permission from Zhang ZM, Basu S. Entropy flow and generation in radiative transfer between surfaces. Int J Heat Mass Transfer 2007;50:702—12, Figure 9.*

The total entropy generation per unit heat transfer is: $(s_{g,1} + s_{g,2})/q_{12} = 1/T_2 - 1/T_1$, which is independent of the emissivity of any surface (Fig. 1.13). The difference between radiation and conduction (or diffusion) heat transfer between two constant-temperature objects is that, in conduction, entropy generation occurs inside the medium (presumably the boundary resistance is negligible). In radiation, on the contrary, entropy generation occurs at the interfaces. The emissivities affect the fraction of entropy generated by individual surfaces, as shown in Fig. 1.13A, where $s_{g,1}/(s_{g,1} + s_{g,2})$ and $s_{g,2}/(s_{g,1} + s_{g,2})$ are plotted in percentages. When both surfaces are black, because $q_{12} = \sigma T_1^4 - \sigma T_2^4$ and $s_{12} = 4/3\sigma T_1^3 - 4/3\sigma T_2^3$, it can easily be verified that 8.1% entropy generation is at surface 1. However, the fraction of entropy generation at surface 1 increases as its emissivity decreases. Assuming surface 2 is black, then $q_{12} = \varepsilon_1\sigma(T_1^4 - T_2^4)$, if s_{12} were also scaled with ε_1, that is $s_{12} = 4/3\varepsilon_1\sigma(T_1^3 - T_2^3)$, the fraction of entropy generation would not change with ε_1 at all. The reason for the redistribution of entropy generation is explained next.

The emitted entropy intensities for surfaces 1 and 2 can be obtained from Eq. (1.25) with

$$X_1 = \frac{\varepsilon_1 I_{\lambda,b1}}{I_\lambda^+} \text{ and } X_2 = \frac{\varepsilon_2 I_{\lambda,b2}}{I_\lambda^-} \tag{1.32}$$

(A)

(B)
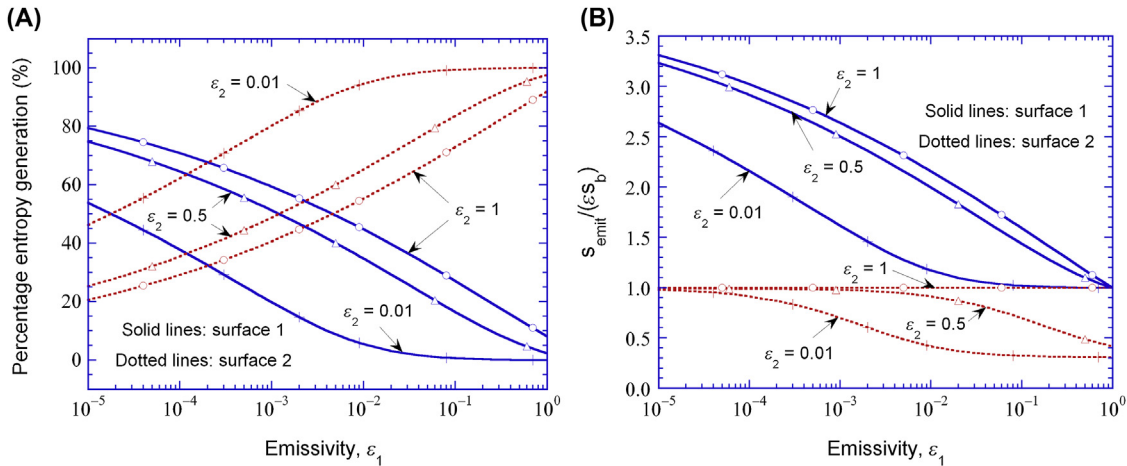
■ **FIGURE 1.13** (A) Percentage entropy generation and (B) the emitted entropy by each surface for $T_1 = 1500$ K and $T_2 = 300$ K. The emitted entropy is normalized to the product of the emissivity and the entropy emitted by a blackbody at the surface temperature. *With permission from Zhang ZM, Basu S. Entropy flow and generation in radiative transfer between surfaces. Int J Heat Mass Transfer 2007;50:702−12, Figure 10.*

respectively. The emitted total entropy flux can be evaluated using $s_{\mathrm{emit}} = \pi \int_0^\infty L_{\lambda,\mathrm{emit}} \, d\lambda$ for each surface under the diffuse assumption. Fig. 1.13B shows the emitted entropy normalized by $4/3\varepsilon\sigma T^3$ for the corresponding surface. It is clear that $4/3\varepsilon\sigma T^3$ does not represent the emitted entropy for either surface. What is more interesting is that the emitted entropy by surface 1 is always greater than (or at least equal to) $4/3\varepsilon_1\sigma T_1^3$, whereas the emitted entropy by surface 2 is always smaller than (or at most equal to) $4/3\varepsilon_2\sigma T_2^3$. Note that the temperature of surface 2 is much lower than that of surface 1 in the numerical example, resulting in a backward flux usually much smaller than the forward flux. When surface 2 is a blackbody, the emission from surface 1 is close to free emission, and the entropy of emission is greater than what would be predicted by $4/3\varepsilon_1\sigma T_1^3$, because the emitted photons do not follow an equilibrium distribution. The increase of the entropy emitted by surface 1 with decreasing ε_1 causes an increase in the net entropy transfer between the two surfaces per unit heat transfer: s_{12}/q_{12}. According to Eq. (1.19), $s_{\mathrm{g},1}/q_{12}$ will increase and $s_{\mathrm{g},2}/q_{12}$ will decrease.

When the emissivity of surface 2 is reduced, a large amount of photons will be reflected back toward surface 1, resulting in an increase of I_λ^+ and a reduction of the entropy associated with the emitted photons with respect to $4/3\varepsilon_1\sigma T_1^3$. At the same time, the reflection increases I_λ^- and subsequently the monochromatic temperature T_λ^-. While the emitted number of photons by surface 2 does not change, the total entropy emitted by surface 2 is reduced. Lowering the $s_{\mathrm{emit},1}/(\varepsilon_1 s_{\mathrm{b}1})$ has a more significant effect in reducing s_{12}/q_{12}. Hence, as ε_2 decreases, for the same ε_1, the fraction of entropy generation by surface 1 decreases and the fraction of entropy generation by surface 2 increases. When one surface is highly reflecting, the photon gas is close to the equilibrium state of the other surface; hence, most of the entropy generation occurs at the highly reflecting surface.

To date, the procedure mentioned above seems to be the only plausible method for the determination of entropy generation and emission by individual surfaces in one of the simplest radiative heat transfer problems. In a direct energy conversion device, the photon energy from a high-temperature source in certain frequency region will be absorbed and converted into electricity rather than thermal energy. It is important to take into account the spectral dependence of the radiative properties of both the emitter and absorber, considering multiple reflections and quantum efficiency of the device. The method presented above should enable such an analysis to be made properly based on the principles of thermodynamics and the physics of thermal radiation.

1.3 **NEAR-FIELD RADIATIVE HEAT TRANSFER**

Having discussed the energy transfer and entropy generation in far-field ra-
diation let us now focus on near-field radiative heat transfer. In this section
we will discuss the fundamentals of near-field radiative heat transfer and try
to understand the differences from far-field radiation. These concepts will
be extended in Chapters 4, 5, 6, and 7 which will discuss theoretical, and
experimental results along with applications of near-field radiation in
different systems.

Let us consider the example of radiative heat transfer between two parallel
plates separated by a vacuum gap of d as in Fig. 1.3. The Stefan−Boltzmann
law predicts the maximum radiative heat flux between two flat plates sepa-
rated by a vacuum to be $\sigma\left(T_1^4 - T_2^4\right)$, where σ is the Stefan−Boltzmann con-
stant and T_1 and T_2 are the temperatures of the two media, respectively. This
law, however, is only applicable when the two emitting/absorbing bodies are
separated by a distance d much greater than the characteristic wavelength of
thermal radiation (λ_T) that can be obtained from Wien's displacement law
[4]. As the distance decreases and becomes comparable with or shorter
than λ_T, near-field effects become important and ray optics can no longer
be used to obtain the energy transfer between the two bodies.

The spacing effect on the net heat transfer arises from two effects that are
interrelated. The first is wave interference that is important when d is close
to but greater than λ_T. In such cases, radiative transfer between two bodies
must be analyzed by considering the wave nature of energy propagation.
An electromagnetic wave emitted from one medium, which is transmitted
to the vacuum gap separating the two bodies, is subject to multiple reflections
inside the gap. The resulting wave interference can be either constructive or
destructive, depending on the phase differences between the multiply reflect-
ing waves. The second spacing effect is due to photon tunneling that contrib-
utes significantly to near-field energy transfer when $d < \lambda_T$. When an
electromagnetic wave traveling in a medium encounters a second medium
which is optically rarer than the first, it experiences total internal reflection
at the interface when the angle of incidence is greater than the critical angle
at the interface. Though the wave is totally reflected inside the first medium,
there exists an evanescent wave in the second medium whose amplitude
decays exponentially from the interface [25,26]. The evanescent wave does
not carry energy in the normal direction since the time average of the Poynt-
ing vector normal to the interface is zero. On the other hand, if a third medium
with refractive index greater than the second medium is brought in close vi-
cinity to the first medium, ie, within the decay length of the forward evanes-
cent wave, the evanescent wave is reflected at the interface between the
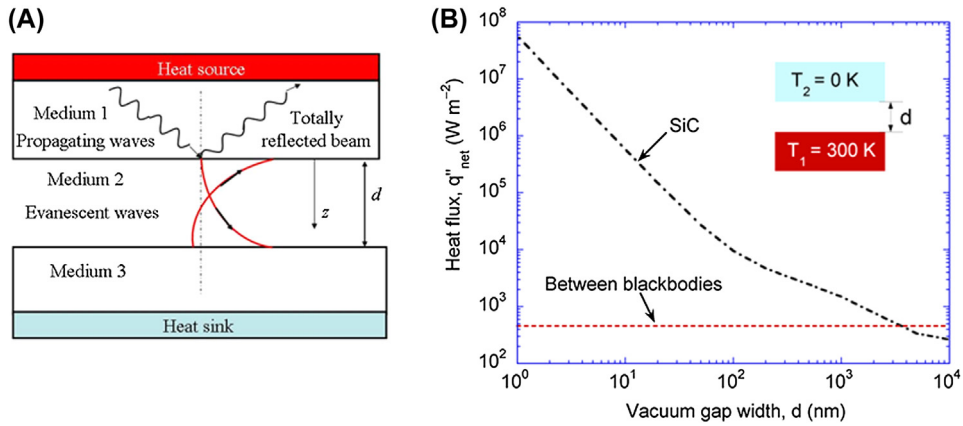
■ **FIGURE 1.14** (A) Schematic illustrating the concept of evanescent waves and photon tunneling; and (B) radiation heat transfer between two SiC plates maintained at 300 and 0 K. The energy transfer between two blackbodies has also been shown for reference. *With permission from Basu S, Zhang ZM, Fu CJ. Review of near-field thermal radiation and its application to energy conversion. Int J Energy Res 2009;33:1203—32, Figure 1.*

second and the third media. The Poynting vector of the coupled evanescent fields has a nonzero normal component, suggesting that energy from the first medium has tunneled through the second medium and reached the third medium. This phenomenon is known as photon tunneling or radiation tunneling, which is responsible for the enhanced energy transfer in the near field [26].

The concept of photon tunneling and evanescent waves is illustrated in Fig. 1.14A where two emitting media (1 and 1) are separated by a vacuum gap, *d*. Fig. 1.14B shows the predicted heat transfer between two SiC plates. The plates are maintained at 300 and 0 K, respectively, and the net heat flux is calculated at different vacuum gaps. For comparison, the heat transfer between two blackbodies maintained at the same temperature as the SiC plates is also plotted. It is observed that the near-field heat transfer between the two SiC plates at 1 nm apart is around five orders of magnitude greater than that between the two blackbodies. Note that at 1 nm vacuum gap, the near-field radiation between SiC plates can be an order of magnitude greater than heat conduction through air at atmospheric pressure.

1.3.1 **Maxwell's Equations**

Thermal radiation between solids is often treated as a surface phenomenon and analyzed using ray optics with the assistance of the concept of emissivity, reflectivity, and absorptivity of the surfaces [4]. On the other hand, radiation heat transfer inside a semitransparent medium is traditionally dealt with by the radiative transfer equation (RTE), considering emission, absorption, and scattering [3,27]. These phenomenological approaches do not fully

account for the origin of thermal emission and break down when wave interference and diffraction become important. Since the wave nature of thermal radiation is neglected while solving the RTE, near-field effects cannot be explained under such a framework. Maxwell's equations describe the propagation of electromagnetic waves and their interactions with matter and hence should be used to analyze the radiative heat transfer between closely spaced bodies. Note that application of Maxwell's equations is not limited to calculation of radiative heat transfer rather they can be applied to any kind of electromagnetic field oscillating at frequency ω. Maxwell's equations provide an interrelationship between the electromagnetic field, source, and material properties. Absorption in Maxwell's equations is accounted for by the imaginary part of the dielectric function also called the extinction coefficient as will be discussed in detail in Chapter 3. Scattering can be explained by these equations by considering the total field as the sum of the incident and scattered fields. However thermal emission, which is a function of the temperature of the medium, is not accounted for in Maxwell's equations. Fluctuational electrodynamics, pioneered by Rytov and coworkers in the 1950s combined the fluctuation-dissipation theorem with Maxwell's equations to fully describe the emission, in both the near and far field [28]. Fluctuation-dissipation theorem will be discussed later in Section 1.3.3.

Maxwell's equations for nonmagnetic media are given by [29].

$$\nabla \times \mathbf{E}(\mathbf{x}, \omega) = i\omega \mathbf{B}(\mathbf{x}, \omega) = i\omega\mu_0 \mathbf{H}(\mathbf{x}, \omega) \quad \text{Faraday's Law} \qquad (1.33a)$$

$$\nabla \times \mathbf{H}(\mathbf{x}, \omega) = -i\omega\varepsilon\mathbf{E}(\mathbf{x}, \omega) \quad \text{Ampere's Law} \qquad (1.33b)$$

$$\nabla \cdot \mathbf{D}(\mathbf{x}, \omega) = \rho_e \quad \text{Gauss's Law} \qquad (1.33c)$$

$$\nabla \cdot \mathbf{B}(\mathbf{x}, \omega) = 0 \quad \text{Gauss's Law} \qquad (1.33d)$$

$$\nabla \cdot \mathbf{J}(\mathbf{x}, \omega) = i\omega\rho_e \quad \text{Continuity Equation} \qquad (1.33e)$$

In the above equations, $\mathbf{E}$ is electric field vector with units V/m, $\mathbf{H}$ is magnetic field vector with units A/m, $\mathbf{D}$ is the electric displacement vector with units C/m^2, $\mathbf{J}$ is electric current density in A/m^2, $\mathbf{B}$ is magnetic flux density in Wb/m^2, and ρ_e is the charge density with units C/m^3. ε and μ_0 are the permittivity of the medium and permeability of vacuum, respectively.

For any material at a temperature above absolute zero, charges such as electrons in metals or ions in polar crystals undergo random thermal motion. The random motion of charges, or dipoles inside the medium represented as ellipses in Fig. 1.15, would result in time-dependent electric currents in the whole space, which in turn generate electric and magnetic fields. However, the electromagnetic waves generated due to charges deep inside the
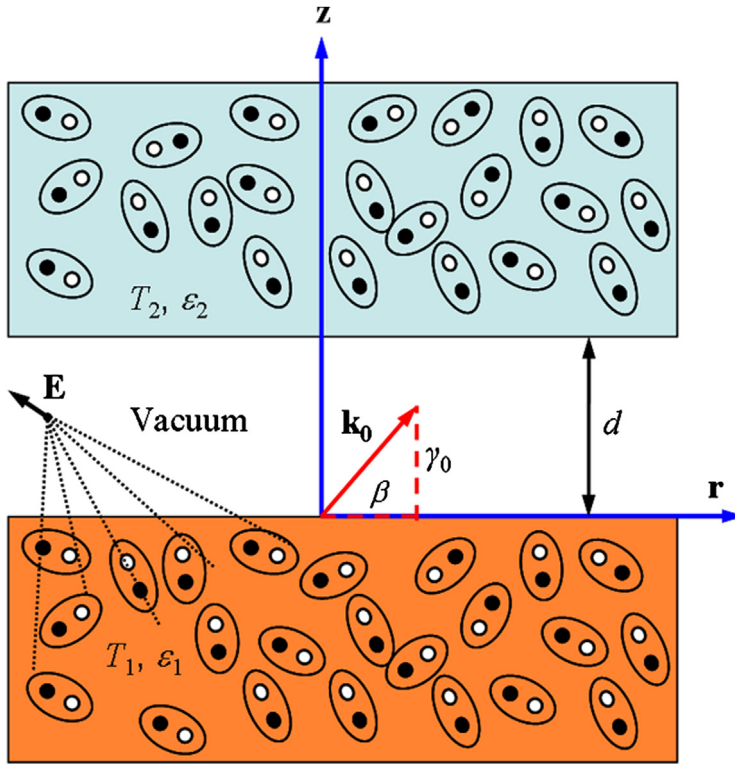
■ **FIGURE 1.15** Schematic for near-field radiation between two closely placed parallel plates at temperatures T_1 and T_2 separated by a vacuum gap of width d. The random motion of the dipoles, represented as ellipses in the figure, result in a space—time-dependent fluctuating electric field. *With permission from Basu S, Zhang ZM, Fu CJ. Review of near-field thermal radiation and its application to energy conversion. Int J Energy Res 2009;33:1203—32, Figure 2(a).*

medium will attenuate due to absorption inside the medium. While the time-average of the induced field is zero at any location and frequency, there exists a nonzero energy density and the resulting electromagnetic waves can carry energy away from the surface. The statistical properties of the electromagnetic field can be fully determined, provided that the statistical properties of the random currents and the transmission properties of the radiation from the emitting medium are known [30]. When dealing with nonmagnetic media, a stochastic current $\mathbf{J}^{x,e}$ is added in Ampère's law in order to model thermal radiation emission due to electric dipole oscillations. For magnetic media, a stochastic current $\mathbf{J}^{x,m}$ should also be included in Faraday's law to model thermal emission due to fluctuating magnetic dipoles [28]. The inclusion of the fluctuating current in Ampere's law makes the Maxwell equations stochastic in nature. In this chapter we will limit our discussion to

nonmagnetic media only for simplicity. Section 4.5 in Chapter 4 devoted to near-field heat transfer in magnetic media or metamaterials which provides the required equations. After the inclusion of the stochastic current term, the modified Ampere's law can be rewritten as

$$\nabla \times \mathbf{H}(\mathbf{x}, \omega) = -i\omega\varepsilon\mathbf{E}(\mathbf{x}, \omega) + \mathbf{J}^x(\mathbf{x}, \omega) \tag{1.34}$$

The current density $\mathbf{J}^x(\mathbf{x},\omega)$ plays the role of a random external source causing thermal fluctuations of the field [31]. The mean value of this random current density, $\langle\mathbf{J}^x(\mathbf{x},\omega)\rangle$, is zero, implying that the mean radiated field is also zero. Note that we have dropped the term e or m in the superscript of current density since we are only considering electric media here.

1.3.2 **Solution of Maxwell's Equations**

While Maxwell's equations can be solved by different methods as will be discussed in Chapter 2, the most commonly adopted method is to express the electric and magnetic fields in terms of Green's function. In this chapter the method of potentials is utilized to solve Maxwell's equations [31]. Let $\mathbf{M}(\mathbf{x},\omega)$ be the magnetic vector potential which satisfies the vector identity $\nabla\cdot(\nabla \times \mathbf{M}(\mathbf{x},\omega)) = 0$. Also the magnetic flux density $\mathbf{B}$ can be written as $\mathbf{B}(\mathbf{x},\omega) = \nabla \times \mathbf{M}(\mathbf{x},\omega)$. Substituting into Faraday's law gives

$$\mathbf{E}(\mathbf{x}, \omega) = i\omega\mathbf{M}(\mathbf{x}, \omega) - \nabla\phi_e \tag{1.35}$$

where ϕ_e is electric scalar potential. Similarly substituting the expression of magnetic flux density in the modified Ampere's law results in the following equation

$$\frac{1}{\mu_0}\nabla \times (\nabla \times \mathbf{M}(\mathbf{x}, \omega)) = \mathbf{J}^x(\mathbf{x}, \omega) + i\omega\varepsilon\nabla\phi_e + \omega^2\varepsilon\mathbf{M}(\mathbf{x}, \omega) \tag{1.36}$$

The Lorentz gauge is then invoked to establish the result between magnetic vector potential and electric scalar potential $\nabla\cdot\mathbf{M}(\mathbf{x},\omega) = i\omega\varepsilon\mu_0\phi_e$. Substituting the Lorentz gauge into Eq. (1.36) results in the well-known Helmholtz equation.

$$(\nabla^2 + k^2)\mathbf{M}(\mathbf{x}, \omega) = -\mu_0\mathbf{J}^x(\mathbf{x}, \omega) \tag{1.37}$$

where $k = \sqrt{\varepsilon\mu_0}\omega$. The magnetic vector potential can then be expressed as

$$\mathbf{M}(\mathbf{x}, \omega) = \mu_0\int_V \mathbf{J}^x(\mathbf{x}, \omega)g(\mathbf{x}, \mathbf{x}', \omega)\, dV \tag{1.38}$$

In Eq. (1.38), $g(\mathbf{x},\mathbf{x}',\omega)$ is the Green's function which is the solution of the field at $\mathbf{x}$ for a point source at $\mathbf{x}'$ described by the Dirac delta function as

$$(\nabla^2 + k^2)g(\mathbf{x}, \mathbf{x}', \omega) = -\delta(|\mathbf{x} - \mathbf{x}'|) \tag{1.39}$$

Eq. (1.38) implies that the field due to source $\mathbf{J}^x(\mathbf{x},\omega)$ is the convolution of the Green's function with that source. The electric and magnetic fields are then given by [32]

$$\mathbf{E}(\mathbf{x},\omega) \;=\; i\omega\mu_0 \int_V dV g(\mathbf{x},\mathbf{x}',\omega) \left[\bar{\bar{\mathbf{I}}} + \frac{1}{k^2}\nabla\nabla\right] \cdot \mathbf{J}^x(\mathbf{x}',\omega) \tag{1.40}$$

$$\mathbf{H}(\mathbf{x},\omega) \;=\; \nabla \times \int_V dV g(\mathbf{x},\mathbf{x}',\omega)\bar{\bar{\mathbf{I}}} \cdot \mathbf{J}^x(\mathbf{x}',\omega) \tag{1.41}$$

$\bar{\bar{\mathbf{I}}}$ is called an idem factor and is a 3×3 matrix [33]. Furthermore, the electric dyadic Green's function is given by the following

$$\bar{\bar{\mathbf{G}}}^e(\mathbf{x},\mathbf{x}',\omega) \;=\; g(\mathbf{x},\mathbf{x}',\omega)\left[\bar{\bar{\mathbf{I}}} + \frac{1}{k^2}\nabla\nabla\right] \tag{1.42a}$$

and the magnetic dyadic Green's function is given by

$$\bar{\bar{\mathbf{G}}}^m(\mathbf{x},\mathbf{x}',\omega) \;=\; \nabla \times \big(g(\mathbf{x},\mathbf{x}',\omega)\bar{\bar{\mathbf{I}}}\big) \tag{1.42b}$$

Consequently, the electric and magnetic fields can be rewritten as

$$\mathbf{E}(\mathbf{x},\omega) \;=\; i\omega\mu_0 \int_V dV \bar{\bar{\mathbf{G}}}^e(\mathbf{x},\mathbf{x}',\omega) \cdot \mathbf{J}^x(\mathbf{x}',\omega) \tag{1.43}$$

$$\mathbf{H}(\mathbf{x},\omega) \;=\; \int_V dV \bar{\bar{\mathbf{G}}}^m(\mathbf{x},\mathbf{x}',\omega) \cdot \mathbf{J}^x(\mathbf{x}',\omega) \tag{1.44}$$

where $\bar{\bar{\mathbf{G}}}^m(\mathbf{x},\mathbf{x}',\omega) = \nabla \times \bar{\bar{\mathbf{G}}}^e(\mathbf{x},\mathbf{x}',\omega)$. Physically the dyadic Green's function (DGF) is a spatial transfer function which links the current density $\mathbf{J}^x(\mathbf{x}',\omega)$ located at $\mathbf{x}'$ inside the emitting media to the field at a location $\mathbf{x}$ outside the emitting volume. The DGF is similar to the scalar Green's function used in the solution of boundary value problems and also in heat conduction. In Eqs. (1.43) and (1.44), the DGF gives a response (field) which is a vector of a source (current density) which is also a vector, as a result of which the DGF is a dyad or a tensor of second rank. Once the electric and magnetic fields are calculated the spectral flux is given by [30]

$$\langle \mathbf{S}(\mathbf{x},\omega) \rangle \;=\; \int_0^\infty \frac{1}{2}\langle \mathrm{Re}[\mathbf{E}(\mathbf{x},\omega) \times \mathbf{H}^*(\mathbf{x},\omega')]\rangle d\omega' \tag{1.45}$$

where $\langle\,\rangle$ represents ensemble averaging, $\mathbf{S}$ is the spectral Poynting vector, ω and ω' are the angular frequencies, and * denotes the complex conjugate. For parallel surfaces separated by vacuum gap d, the electric Green's function is given by [33]

$$\bar{\bar{\mathbf{G}}}^e(\mathbf{x},\mathbf{x}',\omega) \;=\; \frac{i}{8\pi^2} \int d^2\beta \frac{1}{\gamma_1}\left(\hat{\mathbf{s}}t_s^+\hat{\mathbf{s}} + \hat{\mathbf{s}}t_s^-\hat{\mathbf{s}} + \hat{\mathbf{p}}_2^+ t_p^+\hat{\mathbf{p}}_1^+ + \hat{\mathbf{p}}_2^- t_p^-\hat{\mathbf{p}}_1^+\right)e^{-i\gamma_1 z'}e^{i\boldsymbol{\beta}\cdot(r-r')}$$

$$\tag{1.46}$$

where $k_j^2 = (\omega/c)^2 \varepsilon_j = \beta^2 + \gamma_j^2$ and $t_{p(s)}$ are the transmission coefficients for p and s polarization. In r-z-s coordinate, $\widehat{\mathbf{s}} \times \widehat{\mathbf{r}} = \widehat{\mathbf{z}}$, $\widehat{\mathbf{r}} \times \widehat{\mathbf{z}} = \widehat{\mathbf{s}}$, and $\widehat{\mathbf{z}} \times \widehat{\mathbf{s}} = \widehat{\mathbf{r}}$. Also $\mathbf{k}_j^{\pm} = \beta\widehat{\mathbf{r}} \pm \gamma_j\widehat{\mathbf{z}}$ and $\widehat{\mathbf{p}}_j^{\pm} = \widehat{\mathbf{s}} \times \mathbf{k}_j^{\pm}/k_2 = (\beta\widehat{\mathbf{z}} \mp \gamma_j\widehat{\mathbf{r}})/k_j$. Inside the vacuum gap of thickness d,

$$t_p^+(z) = \frac{t_{12}}{1 - r_{23}r_{21}e^{i2\gamma_2 d}}e^{i\gamma_2 z} \text{ and } t_p^-(z) = \frac{t_{12}r_{23}e^{i2\gamma_2 d}}{1 - r_{23}r_{21}e^{i2\gamma_2 d}}e^{-i\gamma_2 z}(0 < z < d)$$

(1.47)

Subscript 1 represents source, 2 represents vacuum gap, and 3 indicates the receiver. The $+$ sign indicates waves in the forward direction, ie, going from medium 1 to 3 and the $-$ sign indicates waves in backward direction, ie, going from medium 3 to 1.

In Eq. (1.46) let $\overline{\overline{e}}(\beta, z) = \frac{1}{\gamma_1}\left(\widehat{\mathbf{s}}t_s^+\widehat{\mathbf{s}} + \widehat{\mathbf{s}}t_s^-\widehat{\mathbf{s}} + \widehat{\mathbf{p}}_2^+t_p^+\widehat{\mathbf{p}}_1^+ + \widehat{\mathbf{p}}_2^-t_p^-\widehat{\mathbf{p}}_1^+\right)$. Hence

$$\overline{\overline{e}}(\beta, z) = \frac{1}{\gamma_1}\left(\widehat{\mathbf{s}}t_s^+\widehat{\mathbf{s}} + \widehat{\mathbf{s}}t_s^-\widehat{\mathbf{s}} + \widehat{\mathbf{p}}_2^+t_p^+\widehat{\mathbf{p}}_1^+ + \widehat{\mathbf{p}}_2^-t_p^-\widehat{\mathbf{p}}_1^+\right)$$

$$= \frac{1}{\gamma_1}\begin{bmatrix} \dfrac{\gamma_2\left(t_p^+ - t_p^-\right)\gamma_1}{k_2 k_1} & -\dfrac{\gamma_2\left(t_p^+ - t_p^-\right)\beta}{k_2 k_1} & 0 \\[3mm] -\dfrac{\beta\left(t_p^+ + t_p^-\right)\gamma_1}{k_2 k_1} & \dfrac{\beta\left(t_p^+ + t_p^-\right)\beta}{k_2 k_1} & 0 \\[3mm] 0 & 0 & t_s^+ + t_s^- \end{bmatrix}$$

(1.48)

The magnetic Green's function is then given by

$$\overline{\overline{\mathbf{G}}}^m(\mathbf{x}, \mathbf{x}', \omega) = \nabla_{\mathbf{x}} \times \overline{\overline{\mathbf{G}}}^e(\mathbf{x}, \mathbf{x}', \omega)$$

$$= -\frac{1}{8\pi^2}\int d^2\beta\,\frac{i}{\gamma_1}\Big((-\beta\widehat{\mathbf{z}} + \gamma_2\widehat{\mathbf{r}})t_s^+\widehat{\mathbf{s}} + (-\beta\widehat{\mathbf{z}} - \gamma_2\widehat{\mathbf{r}})t_s^-\widehat{\mathbf{s}}$$

$$+ k_2\widehat{\mathbf{s}}t_p^+\widehat{\mathbf{p}}_1 + k_2\widehat{\mathbf{s}}t_p^-\widehat{\mathbf{p}}_1\Big)e^{-i\gamma_1 z'}e^{i\boldsymbol{\beta}\cdot(r-r')}$$

(1.49)

Again let $\overline{\overline{\mathbf{h}}}(\beta, z) = \frac{i}{\gamma_1}\Big((-\beta\widehat{\mathbf{z}} + \gamma_2\widehat{\mathbf{r}})t_s^+\widehat{\mathbf{s}} + (-\beta\widehat{\mathbf{z}} - \gamma_2\widehat{\mathbf{r}})t_s^-\widehat{\mathbf{s}} + k_2\widehat{\mathbf{s}}t_p^+\widehat{\mathbf{p}}_1 + k_2\widehat{\mathbf{s}}t_p^-\widehat{\mathbf{p}}_1\Big)$. Accordingly,

$$\overline{\overline{\mathbf{h}}}(\beta, z) = \frac{i}{\gamma_1}\begin{bmatrix} 0 & 0 & \gamma_2\left(t_s^+ - t_s^-\right) \\[3mm] 0 & 0 & -\beta\left(t_s^+ + t_s^-\right) \\[3mm] -\dfrac{k_2\left(t_p^+ + t_p^-\right)\gamma_1}{k_1} & \dfrac{k_2\left(t_p^+ + t_p^-\right)\beta}{k_1} & 0 \end{bmatrix}$$

(1.50)

In *r-z-s* coordinate,

$$
\begin{aligned}
\mathbf{E}(\mathbf{x},\omega) \times \mathbf{H}^*(\mathbf{x},\omega) &= \widehat{\mathbf{r}}\big(E_z H_s^* - E_s H_z^*\big) - \widehat{\mathbf{z}}\big(E_r H_s^* - E_s H_r^*\big) \\
&\quad + \widehat{\mathbf{s}}\big(E_r H_z^* - E_z H_r^*\big)
\end{aligned}
\tag{1.51}
$$

Therefore, basically we need to know $\langle E_l(\mathbf{x},\omega) H_m^*(\mathbf{x},\omega)\rangle$ where l, m could be r, z, or s and $l \neq m$. $E_l(\mathbf{x},\omega) = i\omega\mu_0 \int d^3\mathbf{x}' \overline{\overline{G}}_{lk}^e(\mathbf{x},\mathbf{x}',\omega) J_k(\mathbf{x}',\omega)$ and $H_m^*(\mathbf{x},\omega) = \int d^3\mathbf{x}'' \overline{\overline{G}}_{mn}^{m^*}(\mathbf{x},\mathbf{x}'',\omega) J_n^*(\mathbf{x}'',\omega)$. As a result,

$$
\begin{aligned}
\langle E_l(\mathbf{x},\omega) H_m^*(\mathbf{x},\omega)\rangle &= i\omega\mu_0 \int d^3\mathbf{x}' \int d^3\mathbf{x}'' \, \overline{\overline{G}}_{jk}^e(\mathbf{x},\mathbf{x}',\omega) \overline{\overline{G}}_{mn}^{m^*}(\mathbf{x},\mathbf{x}'',\omega) \\
&\quad \times \langle J_k(\mathbf{x}',\omega) J_n^*(\mathbf{x}'',\omega)\rangle
\end{aligned}
\tag{1.52}
$$

In Eq. (1.52) the only unknown term $\langle J_k(\mathbf{x}',\omega) J_n^*(\mathbf{x}'',\omega)\rangle$ is obtained from the fluctuation dissipation theorem as discussed next.

1.3.3 **Fluctuation Dissipation Theorem**

The stochastic nature of the current density vector results in the average electric and magnetic fields becoming zero. However, as seen from Eq. (1.52), in order to obtain the spectral energy flux, it is important to know the ensemble average of the spatial correlation function of the fluctuating current densities which acts as the source for thermal radiation. The spectral density of the fluctuating currents is related to the local temperature of the body through the fluctuation-dissipation theorem (FDT). The ensemble average of the fluctuating current densities is given by [34]

$$
\langle J_k(\mathbf{x}',\omega) J_n^*(\mathbf{x}'',\omega')\rangle = \frac{4}{\pi}\omega\varepsilon_0 \text{Im}(\varepsilon(\omega))\delta_{mn}\delta(\mathbf{x}'-\mathbf{x}'')\Theta(\omega,T)\delta(\omega-\omega')
\tag{1.53}
$$

where j_m and j_n (m, n = 1, 2, or 3) stands for the *x*, *y*, or *z* component of $\mathbf{J}$, δ_{mn} is the Kronecker delta, and $\delta(\mathbf{x}'-\mathbf{x}'')$ and $\delta(\omega-\omega')$ are the Dirac delta functions. In Eq. (1.53), $\Theta(\omega,T)$ is the mean energy of Planck oscillator at frequency ω in thermal equilibrium and is given by

$$
\Theta(\omega,T) = \frac{\hbar\omega}{\exp(\hbar\omega/k_B T) - 1}
\tag{1.54}
$$

where $\hbar$ is the Planck constant divided by 2π, k_B is the Boltzmann constant, and T is the absolute temperature of the source medium. In Eq. (1.54), the term $1/2\hbar\omega$ that accounts for vacuum fluctuation is omitted since it does not affect the net radiation heat flux. A factor of 4 has been included in Eq. (1.53) to be consistent with the conventional definitions of the spectral energy density and the Poynting vector expressed in Eq. (1.45) since only positive values of frequencies are considered here [24].

Derivations of FDT can be obtained from Refs. [28,35]. The derivation of the FDT has the following underlying assumptions: (1) the bodies are assumed in local thermodynamic equilibrium at an equilibrium temperature T resulting in thermal emission; (2) only isotropic media are considered; (3) the media are nonmagnetic and are defined by a frequency-dependent dielectric function $\varepsilon(\omega)$; and (4) the dielectric function is local in space (ie, the dielectric function is independent of wavefunction). In Eq. (1.53), the Kronecker delta function accounts for the isotropic nature of the medium, Dirac delta function, $\delta(\mathbf{x}' - \mathbf{x}'')$ accounts for the nonlocal form of the dielectric function, and $\delta(\omega - \omega')$ assumes that the fluctuating currents are stationary.

In the extreme proximity (for vacuum gaps less than 1 nm), the dielectric function is not local and its dependence on wavevector must be considered. Recently, Chapuis et al. [36] used two different nonlocal dielectric function models to calculate the near-field heat transfer between two semi-infinite gold plates and compared their results with the heat flux calculated using the Drude model for gold. The heat flux for s polarization is identical for both local and nonlocal dielectric function models. On the other hand, for p polarization, the heat flux predicted using the two different dielectric models starts to differ when the vacuum gap is less than 0.1 nm. While the nonlocal dielectric function saturates the heat flux, using local dielectric function will cause the heat flux to diverge as the vacuum gap $d \to 0$. Chapter 4 includes a separate discussion on the impact of the local form of dielectric function on the near-field heat transfer between parallel surfaces.

Substituting the expression for FDT in Eq. (1.52) results in the following

$$\langle E_l(\mathbf{x}, \omega) H_m^*(\mathbf{x}, \omega) \rangle = \frac{4\mathrm{i}}{\pi} \omega^2 \varepsilon_0 \mu_0 \Theta(\omega, T) \int d^3\mathbf{x}' \overline{\overline{G}}_{jk}^e(\mathbf{x}, \mathbf{x}', \omega) \overline{\overline{G}}_{mn}^{m*}(\mathbf{x}, \mathbf{x}'', \omega)$$

(1.55)

Now, let's focus on the integration $I_{lm} = \int d^3\mathbf{x}' \overline{\overline{G}}_{jk}^e(\mathbf{x}, \mathbf{x}', \omega) \overline{\overline{G}}_{mn}^{m*}(\mathbf{x}, \mathbf{x}'', \omega)$.

$$I_{lm} = \frac{1}{64\pi^4} \int dz' \int d^2\mathbf{r}' \int d^2\boldsymbol{\beta}$$
$$\times \int d^2\boldsymbol{\beta}' \, \overline{\overline{\mathbf{e}}}_{lk}(\beta, z) \overline{\overline{\mathbf{h}}}_{mk}^*(\beta', z) e^{\mathrm{i}(\boldsymbol{\beta}-\boldsymbol{\beta}')\cdot r} e^{2\mathrm{Im}(\gamma_1)z'} e^{-\mathrm{i}(\boldsymbol{\beta}-\boldsymbol{\beta}')\cdot\mathbf{r}'}$$

(1.56)

From the integral representation of Dirac delta function: $\delta(a - a') = \frac{1}{2\pi} \int_{-\infty}^{\infty} e^{\mathrm{i}(a-a')x} \, dx$. It can be obtained that $\int d^2\mathbf{r}' e^{-\mathrm{i}(\boldsymbol{\beta}-\boldsymbol{\beta}')\cdot\mathbf{r}'} = 4\pi^2 \delta(\boldsymbol{\beta} - \boldsymbol{\beta}')$. Therefore,

$$I_{lm} = \frac{1}{16\pi^2} \int dz' \int d^2\boldsymbol{\beta} \, \overline{\overline{e}}_{lk}(\beta, z) \overline{\overline{h}}_{mk}^*(\beta, z) e^{2\mathrm{Im}(\gamma_1)z'}$$
$$= \frac{1}{16\pi^2} \int d^2\boldsymbol{\beta} \, \overline{\overline{e}}_{lk}(\beta, z) \overline{\overline{h}}_{mk}^*(\beta, z) \frac{1}{2\mathrm{Im}(\gamma_1)}$$

(1.57)

where

$$\bar{\bar{\mathbf{e}}}_{lk}(\beta, z)\bar{\bar{h}}_{mk}^{*}(\beta, z)$$

$$= \frac{-i}{\gamma_1\gamma_1^*}\begin{bmatrix} \dfrac{\gamma_2\left(t_p^+ - t_p^-\right)\gamma_1}{k_2 k_1} & -\dfrac{\gamma_2\left(t_p^+ - t_p^-\right)\beta}{k_2 k_1} & 0 \\[3ex] -\dfrac{\beta\left(t_p^+ + t_p^-\right)\gamma_1}{k_2 k_1} & \dfrac{\beta\left(t_p^+ + t_p^-\right)\beta}{k_2 k_1} & 0 \\[3ex] 0 & 0 & t_s^+ + t_s^- \end{bmatrix}\begin{bmatrix} 0 & 0 & -\dfrac{k_2^*\left(t_p^+ + t_p^-\right)^*\gamma_1^*}{k_1^*} \\[3ex] 0 & 0 & \dfrac{k_2^*\left(t_p^+ + t_p^-\right)^*\beta}{k_1^*} \\[3ex] \gamma_2^*\left(t_s^+ - t_s^-\right)^* & -\beta\left(t_s^+ + t_s^-\right)^* & 0 \end{bmatrix}$$

$$= \frac{-i}{\gamma_1\gamma_1^*}\begin{bmatrix} 0 & 0 & -\dfrac{\gamma_2 k_2^*\left(t_p^+ - t_p^-\right)\left(t_p^+ + t_p^-\right)^*\left(\gamma_1\gamma_1^* + \beta^2\right)}{k_2 k_1 k_1^*} \\[4ex] 0 & 0 & \dfrac{\beta k_2^*\left(t_p^+ + t_p^-\right)\left(t_p^+ + t_p^-\right)^*\left(\gamma_1\gamma_1^* + \beta^2\right)}{k_2 k_1 k_1^*} \\[4ex] \gamma_2^*\left(t_s^+ + t_s^-\right)\left(t_s^+ - t_s^-\right)^* & -\beta\left(t_s^+ + t_s^-\right)\left(t_s^+ + t_s^-\right)^* & 0 \end{bmatrix}$$

$$(1.58)$$

In the vacuum gap ($\varepsilon_2 = 1$), $k_2 = k_2^* = \omega/c$. Therefore, the r and z components of Poynting vector are given by the following,

$$S_r(z) = \frac{\Theta(\omega, T)}{\pi^2}\int_0^\infty \frac{\mathrm{Re}(\gamma_1)}{4\gamma_1\gamma_1^*}\left(\beta\left(t_s^+ + t_s^-\right)\left(t_s^+ + t_s^-\right)^* \right.$$

$$\left. + \beta\left(t_p^+ + t_p^-\right)\left(t_p^+ + t_p^-\right)^*\frac{\left(\gamma_1\gamma_1^* + \beta^2\right)}{k_1 k_1^*}\right)\beta\,d\beta \qquad (1.59)$$

$$S_z(z) = \frac{\Theta(\omega, T)}{\pi^2}\int_0^\infty \frac{\mathrm{Re}(\gamma_1)}{4\gamma_1\gamma_1^*}\left(\mathrm{Re}\left[\gamma_2^*\left(t_s^+ + t_s^-\right)\left(t_s^+ - t_s^-\right)^*\right]\right.$$

$$\left. + \mathrm{Re}\left[\gamma_2\left(t_p^+ - t_p^-\right)\left(t_p^+ + t_p^-\right)^*\right]\frac{\left(\gamma_1\gamma_1^* + \beta^2\right)}{k_1 k_1^*}\right)\beta\,d\beta \qquad (1.60)$$

The reflection and transmission Fresnel coefficient are based on the electric field as:

$$r_{lm} = \frac{\gamma_l/\varepsilon_l - \gamma_m/\varepsilon_m}{\gamma_l/\varepsilon_l + \gamma_m/\varepsilon_m} \quad \text{and} \quad t_{lm} = \frac{2\gamma_l/\sqrt{\varepsilon_l\varepsilon_m}}{\gamma_l/\varepsilon_l + \gamma_m/\varepsilon_m} \qquad (1.61)$$

Note that these expressions for Poynting vector are for heat flux calculations inside the vacuum gap. Chapters 4 and 5 present results for near-field heat transfer calculated between different geometries and materials.

1.3.4 **Density of States in Near-Field Radiation**

After calculating the spectral heat flux, the next objective is to calculate the spectral energy density in the vacuum gap during near-field heat transfer between two parallel surfaces. The spectral energy density in the vacuum space between the two semi-infinite surfaces is given by [34]

$$\langle u(\mathbf{x}, \omega) \rangle = \int_0^\infty \frac{\varepsilon_0}{4} \langle \mathbf{E}(\mathbf{x}, \omega) \cdot \mathbf{E}^*(\mathbf{x}, \omega') \rangle + \frac{\mu_0}{4} \langle \mathbf{H}(\mathbf{x}, \omega) \cdot \mathbf{H}^*(\mathbf{x}, \omega') \rangle \, d\omega' \quad (1.62)$$

The spectral energy density can be looked upon as the electromagnetic energy per unit volume per unit angular frequency. It is the product of the local density of states (LDOS), $D(z,\omega)$, and the mean energy of the Planck oscillator, ie,

$$\langle u(z, \omega) \rangle = D(z, \omega) \Theta(\omega, T) \quad (1.63)$$

The LDOS is the number of modes per unit frequency interval per unit volume. It is a fundamental quantity and can provide a qualitative understanding of the enhanced near-field radiation. In Eq. (1.63), the LDOS is expressed as a function of z only due to the continuous translation symmetry of the system in the radial direction. Several studies have discussed the LDOS for a free-emitting surface, ie, without medium 3 [24,34]. Basu et al. [30] developed an expression for LDOS in the vacuum gap by considering multiple reflections from the receiver. Neglecting the emission from the receiver, the LDOS can be expressed as the sum of electric and magnetic density of states; thus,

$$D(z, \omega) = D_E(z, \omega) + D_M(z, \omega) \quad (1.64)$$

It can be shown that

$$D_E(z, \omega) = \frac{\omega \text{Im}(\varepsilon_1)}{16\pi^2 c^2} \int_0^\infty \left[\left(|\gamma_2 t_1^p|^2 + |\beta t_3^p|^2 \right) \frac{\beta^2 + \gamma_1 \gamma_1^*}{k_1 k_1^*} \right.$$
$$\left. + |k_2 t_3^s|^2 \right] \frac{\beta}{|\gamma_1|^2 \text{Im}(\gamma_1)} \, d\beta \quad (1.65a)$$

and

$$D_M(z, \omega) = \frac{\omega \text{Im}(\varepsilon_1)}{16\pi^2 c^2} \int_0^\infty \left(|k_2 t_3^p|^2 \frac{\beta^2 + \gamma_1 \gamma_1^*}{k_1 k_1^*} + |\gamma_3 t_1^s|^2 \right.$$
$$\left. + |\beta t_3^s|^2 \right) \frac{\beta}{|\gamma_1|^2 \text{Im}(\gamma_1)} \, d\beta \quad (1.65b)$$

In the above expressions, $t_1 = t_+ - t_-$ and $t_3 = t_+ + t_-$, where

$$t_+ = \frac{t_{12} e^{i\gamma_2 z}}{1 - r_{23} r_{21} e^{i2\gamma_2 d}} \quad (1.66a)$$

and

$$t_- = \frac{t_{12} r_{23} e^{i2\gamma_2(d-z)}}{1 - r_{23} r_{21} e^{i2\gamma_2 d}} \tag{1.66b}$$

where $t_{12} = 1 + r_{12}$ is the Fresnel transmission coefficient for a given polarization [26] and d is the thickness of the vacuum gap. Note that subscripts $+$ and $-$ represent the forward and backward waves (due to multiple reflections from both surfaces), respectively, in the vacuum gap while the superscripts indicate the two different porlarizations. As seen from Eqs. (1.65a) and (1.65b), the density of states is a function of the material properties of the emitter and the receiver which are temperature-dependent. As a result, LDOS is an implicit function of temperature. Density of states for near-field radiation between doped silicon plates has been calculated in Chapter 4 based on Eqs. (1.65a) and (1.65b).

1.4 **ENTROPY GENERATION IN NEAR-FIELD THERMAL RADIATION**

In Section 1.2, while discussing entropy generation and transfer in radiative heat transfer, we had neglected any near-field effects like photon tunneling and evanescent waves. In this section we will discuss the entropy generation during near-field thermal radiation utilizing expressions for density of states as defined in Section 1.3. Dorofoyev [37] was the first to provide expressions for spectral entropy density for free emission from a surface for both propagating and evanescent waves using the concept of density of states. Previous studies while calculating the entropy of thermal radiation in the far-field assumed that the local density of states and velocity of radiation are independent of position and are given by their values in free space. These assumptions break down when near-field effects are present. Dorofeyev's work was the first study which considered the effect of position in the calculation of spectral entropy density. The expressions for spectral entropy density which are valid only in local equilibrium for propagating and evanescent waves are given by the following [37]

$$S_{\text{prop}}(z, T) = \int_0^\infty \rho_{\text{prop}}(\omega, z) \frac{\partial}{\partial T} \{ k_{\text{B}} T \ln[Z(\omega, T)] \} \, d\omega \tag{1.67a}$$

$$S_{\text{evan}}(z, T) = \int_0^\infty \rho_{\text{evan}}(\omega, z) \frac{\partial}{\partial T} \{ k_{\text{B}} T \ln[Z(\omega, T)] \} \, d\omega \tag{1.67b}$$

In Eq. (1.67) the subscripts "prop" and "evan" refer to propagating and evanescent waves, respectively. ρ denotes the density of states that can be

obtained from Eq. (1.65) by considering free emission into vacuum. $Z(\omega,T)$ is the partition function given by the following

$$Z(\omega, T) = \frac{\exp(-\hbar\omega/2k_B T)}{1 - \exp(-\hbar\omega/k_B T)} \qquad (1.68)$$

While the expressions for spectral entropy density in Ref. [37] are applicable only for equilibrium conditions, Narayanaswamy and Zheng [38] derived expression for entropy density for near-field thermal radiation between two multilayer structures in the vacuum cavity separating them without any assumption for equilibrium conditions. In Ref. [38] the expression for polarization-dependent entropy density at a given distance z inside the vacuum gap is given by

$$s^j(\mu, z) = k_B \rho^j(\mu, z) \left[\left(1 + \frac{n^j(\mu, z)}{\rho^j(\mu, z)} \right) \ln\left(1 + \frac{n^j(\mu, z)}{\rho^j(\mu, z)} \right) \right.$$
$$\left. - \left(\frac{n^j(\mu, z)}{\rho^j(\mu, z)} \right) \ln\left(\frac{n^j(\mu, z)}{\rho^j(\mu, z)} \right) \right] \qquad (1.69)$$

Notice the similarity of Eq. (1.69) with Eq. (1.14). In Eq. (1.69) μ indicates the space containing the microscopic states into which the photons are distributed due to near-field effects, n represents the number of photons per unit volume, j is the polarization state, and ρ is the density of states. Expressions for n and μ depend on the geometry of the structure under consideration. The spectral energy density is related to n and μ by the following

$$u^j(z) = \int_{PW} d\mu \hbar\omega n^j(\mu, z) + \int_{EW} d\mu \hbar\omega n^j(\mu, z) \qquad (1.70)$$

In Eq. (1.70), PW and EW signify propagating and evanescent waves, respectively. For the structure shown in Fig. 1.16 the expressions for n are provided by the following

$$n_1(\mu, z) = \begin{cases} \dfrac{(1/8\pi^3)\mathrm{sgn}(k_{z0})}{(e^{\hbar\omega/k_B T_1} - 1)} \dfrac{\left(1 - \left|R_1^j k_{z0}\right|^2\right)\left[1 + \left|R_2^j k_{z0}\right|^2 + \left(\frac{k_\rho}{k_0}\right)^2 2Re\left(R_2^j k_{z0} e^{i2k_{z0}(z_2-z)}\right)\right]}{\left|1 - R_1^j k_{z0} R_2^j k_{z0} e^{i2k_{z0}d}\right|^2} & \text{for PW} \\[3em] \dfrac{(1/8\pi^3)\mathrm{sgn}(\beta_{z0})}{(e^{\hbar\omega/k_B T_1} - 1)} \dfrac{k_0}{\sqrt{\beta_{z0}^2 + k_\rho^2}} \dfrac{2\mathrm{Im}\left(R_1^j \beta_{z0}\right) e^{-2\beta_{z0}d}}{\left|1 - R_1^j \beta_{z0} R_2^j \beta_{z0} e^{-2\beta_{z0}d}\right|^2} & \text{for EW} \\[2em] \times \left[2Re\left(R_2^j \beta_{z0}\right) + \left(\frac{k_\rho}{k_0}\right)^2 \left(e^{2\beta_{z0}(z_2-z)} + e^{-2\beta_{z0}(z_2-z)}\left|R_2^j \beta_{z0}\right|^2\right)\right] \end{cases} \qquad (1.71a)$$
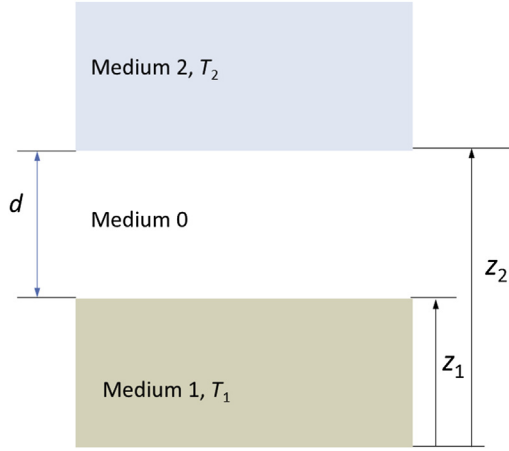
■ **FIGURE 1.16** Schematic for near-field heat transfer between two semi-infinite media separated by a vacuum gap.

$$
n_2(\mu,z) =
\begin{cases}
\dfrac{(1/8\pi^3)\mathrm{sgn}(k_{z0})}{(e^{\hbar\omega/k_B T_2}-1)}\dfrac{\left(1-\left|R_2^j k_{z0}\right|^2\right)\left[1+\left|R_1^j k_{z0}\right|^2+\left(\dfrac{k_\rho}{k_0}\right)^2 2\mathrm{Re}\left(R_1^j k_{z0}e^{i2k_{z0}(z-z_1)}\right)\right]}{\left|1-R_1^j k_{z0}R_2^j k_{z0}e^{i2k_{z0}d}\right|^2} & \text{for PW}\\[20pt]
\dfrac{(1/8\pi^3)\mathrm{sgn}(\beta_{z0})}{(e^{\hbar\omega/k_B T_2}-1)}\dfrac{k_0}{\sqrt{\beta_{z0}^2+k_\rho^2}}\dfrac{2\mathrm{Im}\left(R_2^j \beta_{z0}\right)e^{-2\beta_{z0}d}}{\left|1-R_1^j \beta_{z0}R_2^j \beta_{z0}e^{-2\beta_{z0}d}\right|^2}\\[20pt]
\qquad\times\left[2\mathrm{Re}\left(R_1^j \beta_{z0}\right)+\left(\dfrac{k_\rho}{k_0}\right)^2\left(e^{2\beta_{z0}(z-z_1)}+e^{-2\beta_{z0}(z-z_1)}\left|R_1^j \beta_{z0}\right|^2\right)\right] & \text{for EW}
\end{cases}
$$

$$(1.71b)$$

In Eqs (1.71a) and (1.71b) T_1 and T_2 are the temperature of the two media. R_1 and R_2 are the Fresnel reflection coefficients of the two media. Needless to say if the two media are identical then R_1 and R_2 are same and $n_1(\mu,z) = n_2(\mu,z)$. For propagating waves, $k_\rho^2+k_{z0}^2 = k_0^2$ and $k_\rho^2-\beta_{z0}^2 = k_0^2$ for evanescent waves.

The entropy flux is then given by

$$
S^j(z) = \int d\mu s^j(\mu,z)v_{e,r}^j(\mu,z) \tag{1.72}
$$

$v_{e,r}^j(\mu,z)$ is the z component of the polarization-dependent local velocity of photon energy transmission. For evanescent waves, $v_{e,r}^j(\mu,z)$ is given by [38]

$$v_{e,r}^{j}(\mu, z) = \frac{\dfrac{c\beta_{z0}k_0}{k_\rho^2}\dfrac{2\mathrm{Im}[R_{0x}|\beta_{z0}|]e^{-2\beta_{z0}z_x}}{1 + |R_{0x}|\beta_{z0}||^2 e^{-4\beta_{z0}z_x}}}{1 + \left(\dfrac{k_\rho}{k_0}\right)^{-2}\dfrac{2\mathrm{Re}[R_{0x}|\beta_{z0}|]e^{-2\beta_{z0}z_x}}{1 + |R_{0x}|\beta_{z0}||^2 e^{-4\beta_{z0}z_x}}} \tag{1.73}$$

Here the subscript $x = (1, 2)$ when $r = (2, 1)$.

Next we calculate the ideal work and efficiency for near-field thermal radiation. Let us consider the near-field heat transfer between two parallel plates at temperature T_h and T_e separated by vacuum gap, d with $T_h > T_e$. For simplicity we assume that the environment temperature is also T_e. The maximum available work that can be obtained from this system is

$$\dot{W} = T_e \Delta \dot{S} - \Delta \dot{Q} \tag{1.74}$$

In the above equation, $\Delta \dot{S}$ is variation of the entropy flux and $\Delta \dot{Q}$ is the variation of the energy flux due to near-field heat transfer. Efficiency is then given by the ratio of the available work to the input energy flux, ie,

$$\eta = \frac{\dot{W} - T_e \Delta \dot{S}_{irr}}{\dot{Q}(T_h)} \tag{1.75}$$

$\Delta \dot{S}_{irr}$ is the variation in the entropy generation due to irreversibilities in the system. The upper bound of efficiency is given for a reversible system when $\Delta \dot{S}_{irr} = 0$ and is given by

$$\eta_u = \frac{\dot{W}}{\dot{Q}(T_h)} \tag{1.76}$$

Based on the entropy flux and energy flux expressions provided it is possible to calculate the upper limit for efficiency during near-field heat transfer. For reference η_u for blackbody radiation is given by [39]

$$\eta_{u,bb} = 1 - \frac{4}{3}\frac{T_e}{T_h} + \frac{1}{3}\left(\frac{T_e}{T_h}\right)^4 \tag{1.77}$$

1.5 **CONCLUSION**

This chapter presents the fundamentals of heat transfer before discussing near-field thermal radiation. The discussion on the different heat transfer modes has been restricted to a very elementary level without getting into details as can be found in classical heat transfer textbooks. We have investigated entropy generation and flow in far-field radiation heat transfer since none of the available textbooks or publications provides detailed and unambiguous second law analysis for radiation heat transfer. With the help of different examples and case studies we have shown how entropy emitted and generated at each surface can be evaluated using expressions that are

consistent with nonequilibrium thermodynamics. A significant section of this chapter is devoted toward the introduction of near-field thermal radiation to the readers. We have highlighted the differences in near-field and far-field thermal radiation heat transfer. Important concepts such as photon tunneling and evanescent waves, which are central toward understanding of near-field thermal radiation, have been discussed. These definitions, along with several other concepts introduced in this chapter, will be referenced to throughout this textbook. We have also derived expressions for Poynting vector from Maxwell's equations using Green's function formalism for near-field heat transfer between two parallel plates. In the concluding section of this chapter we have discussed thermodynamics of near-field thermal radiation and derived expressions for entropy generation and second law efficiency. This chapter should therefore serve as the introduction to near-field thermal radiation and provide the required background on which more complex concepts related to nanoscale radiation can be discussed in the subsequent chapters.

REFERENCES

[1] Incropera FP, DeWitt DP. Fundamentals of heat and mass transfer. 5th ed. New York: Wiley; 2002.
[2] Prasher R. Graphene spreads the heat. Science 2010;328:185−6.
[3] Modest MF. Radiative heat transfer. 2nd ed. San Diego: Academic Press; 2003.
[4] Siegel R, Howell JR. Thermal radiation heat transfer. New York: Taylor and Francis; 2002.
[5] Planck M. The theory of heat radiation. New York: Dover Publications; 1959.
[6] Zhang ZM, Basu S. Entropy flow and generation in radiative transfer between surfaces. Int J Heat Mass Transf 2007;50:702−12.
[7] Planck M. On the law of distribution of energy in the normal spectrum. Ann Phys 1901;553−63.
[8] Essex C, Kennedy DC, Berry RS. How hot is radiation? Am J Phys 2003;71: 969−78.
[9] Petela R. Exergy of heat radiation. J Heat Transf 1964;86:187−92.
[10] Petela R. Exergy of undiluted thermal radiation. Sol Energy 2003;74:469−88.
[11] Jeter SM. Maximum conversion efficiency for the utilization of direct solar radiation. Sol Energy 1981;26:231−6.
[12] Gribik A, Osterle JF. The second law efficiency of solar energy conversion. J Sol Energy 1984;106:16−21.
[13] Bejan A. Advanced engineering thermodynamics. 2nd ed. New York: Wiley; 1997.
[14] Arpaci VS. Radiation entropy production-heat lost to entropy. Adv Heat Transf 1991; 21:239−76.
[15] Landsberg PT, Tonge G. Thermodynamics of the conversion of diluted radiation. J Phys A 1979;12:551−61.
[16] Landsberg PT, Tonge G. Thermodynamic energy conversion efficiencies. J Appl Phys 1980;51:R1−20.

[17] Wright SE, Scott DS, Haddow JB, Rosen MA. On the entropy of radiative transfer in engineering thermodynamics. Int J Eng Sci 2001;39:1691−706.

[18] Whale MD. Effective flux temperature formulation for energy conversion using microscale thermal radiation. New York: International Mechanical Engineering Congress and Exposition; November 2001. Paper No. HTD-24275.

[19] Caldas M, Semiao V. Entropy generation through radiative transfer in participating media: analysis and numerical computation. J Quant Spectrosc Radiat Transf 2005; 96:423−37.

[20] Liu LH, Chu SX. On the entropy generation formula of radiation heat transfer processes. J Heat Transf 2006;128:504−6.

[21] Zhang ZM. Surface temperature measurement using optical techniques. Ann Rev Heat Transf 2000;11:351−411.

[22] Mandel L, Wolf E. Optical coherence and quantum optics. Cambridge: Cambridge University Press; 2005.

[23] Gyftopoulos EP, Beretta GP. Thermodynamics: foundations and applications. New York: Macmillan; 1991.

[24] Fu CJ, Zhang ZM. Nanoscale radiation heat transfer for silicon at different doping levels. Int J Heat Mass Transf 2006;49:1703−18.

[25] Cravalho EG, Tien CL, Caren RP. Effect of small spacings on radiative transfer between two dielectrics. J Heat Transf 1967;89:351−8.

[26] Zhang ZM. Nano/Microscale heat transfer. New York: McGraw-Hill; 2007.

[27] Chandrasekhar S. Radiative transfer. New York: Dover; 1960.

[28] Rytov SM, Krastov YA, Tatarskii VI. Principles of statistical radiophysics. New York: Springer-Verlag; 1987.

[29] Griffiths DJ. Introduction to electrodynamics. New Jersey: Prentice Hall; 1999.

[30] Basu S, Lee BJ, Zhang ZM. Near-field radiation calculated with an improved dielectric function model for doped silicon. J Heat Transf 2010;132:023302.

[31] Francoeur M, Menguc MP. Role of fluctuational electrodynamics in near-field radiative heat transfer. J Quant Spectrosc Radiat Transf 2008;109:280−93.

[32] Tai CT. Dyadic green functions in electromagnetic theory. New York: IEEE Press; 1994.

[33] Sipe JE. New Green-function formalism for surface optics. J Opt Soc Am B 1987;4: 481−9.

[34] Joulain K, Mulet J-P, Marquier F, Carminati R, Greffet J-J. Surface electromagnetic waves thermally excited: radiative heat transfer, coherence properties and Casimir forces revisited in the near field. Surf Sci Rep 2005;57:59−112.

[35] Landau LD, Lifshitz EM. Electrodynamics of continuous media. Reading: Addison-Wesley; 1960.

[36] Chapuis PO, Volz S, Henkel C, Joulain K, Greffet JJ. Effects of spatial dispersion in near-field radiative heat transfer between two parallel metallic surfaces. Phys Rev B 2008;77:035431.

[37] Dorofoyev I. Thermodynamic functions of fluctuating electromagnetic fields within a heterogeneous system. Phys Scripta 2011;84:055003.

[38] Narayanaswamy A, Zheng Y. Theory of thermal nonequilibrium entropy in near-field thermal radiation. Phys Rev B 2013;88:075412.

[39] Latella I, Perez-Madrid A, Lapas LC. Miguel Rubi J. Near-field thermodynamics: useful work, efficiency, and energy harvesting. J Appl Phys 2014;115:124307.